

## Tracking X-ray Variability in Next Generation EHT LLAGN Targets

NICOLE M. FORD <sup>1,2</sup> MICHAEL NOWAK <sup>3</sup> VENKATESH RAMAKRISHNAN <sup>4,5</sup> DARYL HAGGARD <sup>1,2</sup>  
KRISTEN DAGE <sup>6</sup> DHANYA G. NAIR <sup>7,8</sup> AND CHI-KWAN CHAN <sup>9,10,11</sup>

<sup>1</sup>*Department of Physics, McGill University, 3600 rue University, Montreal, Québec, H3A 2T8, Canada*

<sup>2</sup>*Trottier Space Institute, 3550 Rue University, Montréal, Québec, H3A 2A7, Canada*

<sup>3</sup>*Dept. of Physics, Washington University in Saint Louis, MSC 1105-109-02, One Brookings Drive, St. Louis, MO 63130-4899*

<sup>4</sup>*Finnish Centre for Astronomy with ESO, FI-20014 University of Turku, Finland*

<sup>5</sup>*Aalto University Metsähovi Radio Observatory, Metsähovintie 114, FI-02540 Kylmäälä, Finland*

<sup>6</sup>*International Centre for Radio Astronomy Research – Curtin University, GPO Box U1987, Perth, WA 6845, Australia*

<sup>7</sup>*Astronomy Department, Universidad de Concepción, Casilla 160-C, Concepción, Chile*

<sup>8</sup>*Max Planck Institute for Radio Astronomy, Auf dem Hügel 69, 53121 Bonn, Germany*

<sup>9</sup>*Steward Observatory and Department of Astronomy, University of Arizona, 933 N. Cherry Ave., Tucson, AZ 85721, USA*

<sup>10</sup>*Data Science Institute, University of Arizona, 1230 N. Cherry Ave., Tucson, AZ 85721, USA*

<sup>11</sup>*Program in Applied Mathematics, University of Arizona, 617 N. Santa Rita, Tucson, AZ 85721, USA*

### ABSTRACT

1 We present a 5 month *NICER* X-ray monitoring campaign for two low luminosity active galactic  
2 nuclei (LLAGNs) – NGC 4594 and IC 1459 – with complementary *Swift* and *NuSTAR* observations.  
3 Utilizing an absorbed power law and thermal source model combined with *NICER*'s SCORPEON  
4 background model, we demonstrate the effectiveness of joint source/background modeling for constraining  
5 emission from faint, background-dominated targets. Both sources are dominated by nuclear power law  
6 emission with photon indices  $\Gamma \sim 1.5 - 2$ , with NGC 4594 being slightly harder than IC 1459. The  
7 thermal contribution in both sources is fainter, but constant, with  $kT \sim 0.5$  keV ( $\sim 5 \times 10^6$  K). The  
8 power law flux and  $\Gamma$  are strongly anti-correlated in both sources, as has been seen for other LLAGNs  
9 with radiatively inefficient accretion flows. NGC 4594 is the brighter source and exhibits significant  
10 aperiodic variability. Its variability timescale with an upper limit of 5 – 7 days indicates emission  
11 originating from  $< 100 r_g$ , at the scale of the inner accretion flow. A spectral break found at  $\sim 6$  keV,  
12 while tentative, could arise from synchrotron/inverse compton emission. This high-cadence LLAGN  
13 X-ray monitoring campaign underlines the importance of multi-wavelength variability studies for a  
14 sample of LLAGNs to truly understand their accretion and outflow physics.

### 1. INTRODUCTION

In active galactic nuclei (AGNs), the accretion and feedback from the central supermassive black hole (SMBH) directly impact the host galaxy. The brightest AGNs, known as quasars/QSOs and blazars, have been extensively surveyed (see e.g., Khachikian & Weedman 1974; Schmidt 1963; Richards et al. 2006). These systems are thought to have a thin disk configuration (Shakura & Sunyaev 1973). Standard thin disks are optically thick and radiatively efficient, so heat can be radiated away and generate a bright nuclear region. There is evidence, however, that SMBH activity undergoes cyclical “flickering”, oscillating between lower and higher accretion/emission states (Di Matteo et al. 2005; Greene & Ho 2007; Schawinski et al. 2015). AGNs with low accretion rates and thus luminosities are hereafter referred to as low luminosity AGNs (LLAGNs). LLAGNs

have typical bolometric luminosities ( $L_{\text{bol}}$ ) below  $10^{42}$  erg s<sup>-1</sup> ( $10^9 L_{\odot}$ ), as a result of accreting at  $< 0.01$  times the Eddington luminosity ( $L_{\text{Edd}}$ ). These may actually represent the most common state of AGN activity; some form of LLAGN is thought to exist in  $\sim 1/3$  of all galaxies in the local Universe ( $z \approx 0$ ; Ho 2008). Understanding LLAGN accretion and feedback is therefore essential to interpreting the evolution of both SMBHs and their host galaxies.

In LLAGNs, the inner accretion disk is likely a radiatively inefficient accretion flow (RIAF; Narayan 2002). A RIAF is optically thin, geometrically thick, and contains a quasi-spherical inflow in the innermost tens of gravitational radii ( $r_g = 2GM/c^2$ ). The astrophysical community is actively pursuing emission signatures that distinguish LLAGNs as being in a RIAF state (e.g., Yuan et al. 2003; Nemmen et al. 2006; Ho 2009; Best &

Heckman 2012; She et al. 2018; Jana et al. 2023). Meanwhile, a correlation has been observed between low accretion rate and jet-dominated emission (see Nagar et al. 2005; Ho 2008 and references therein). In RIAF systems, a substantial fraction of the gravitational energy is released kinetically through jets and outflows, for example via the Blandford-Znajek mechanism (Blandford & Znajek 1977). The relative contribution to the emission in the inner 100s of  $r_g$  from a RIAF versus a jet is a matter of active debate (e.g., Narayan 1996; Markoff et al. 2007; Event Horizon Telescope Collaboration et al. 2019; Fernández-Ontiveros et al. 2023; Ruffa et al. 2024), with observers seeking ways of disentangling the two.

The broadband spectral energy distributions (SEDs) of LLAGNs have several distinct features, presumably related to their RIAF and/or jet emission. They tend to be bright in centimeter to radio frequencies (see summary in Ho 2008). They show a steep power law continuum extending from the infrared (IR)/optical to the ultraviolet (UV) (e.g., Willner et al. 1985; Halpern & Eracleous 1994; Fernández-Ontiveros et al. 2023). LLAGNs do not have the expected optical/UV “blue bump”, which is the characteristic spectral signature of thermal emission from the accretion disk (Chiaberge et al. 2006; Ho 2008; Younes et al. 2012).

In the X-ray, LLAGNs can show a thermal bump below 2 keV. This bump may arise from some combination of star formation processes (e.g., González-Martín et al. 2009; Falocco et al. 2020; Diaz et al. 2023), a hot interstellar medium (e.g., Kim et al. 2019; Younes et al. 2019; Diaz et al. 2023), and/or warm Comptonisation of a truncated standard accretion disk located at 10s - 100s of  $r_g$  (e.g., Kubota & Done 2018; Younes et al. 2019; Falocco et al. 2020). Emission above 2 keV follows a power law shape (e.g., Ho et al. 2001; Donato et al. 2004; Ho 2008; González-Martín et al. 2006, 2009, 2016; She et al. 2018; Fernández-Ontiveros et al. 2023). The shape originates from accelerated leptons within the jets and/or the inner accretion flow that Comptonize either locally-produced photons (synchrotron self-Compton; SSC) or externally-produced photons (for further details see e.g., Dermer et al. 1992; Sikora et al. 1994; Hopkins et al. 2009; Prieto et al. 2016; Bandyopadhyay et al. 2019). LLAGNs lack the relativistic iron reflection lines associated with X-ray emission from, for example, typical Seyfert I disks (see e.g., Ptak et al. 2004; Kawamuro et al. 2013). The absence of both relativistic X-ray reflection and optical/UV thermal disk emission has been taken as evidence for LLAGNs being in a RIAF state, potentially with a truncated standard disk (see e.g., the RIAF models of M81\* in Young et al. 2007, 2018). More multi-wavelength observations of a

sample of LLAGNs are necessary to fill in the details of this departure from the standard AGN disk structure.

In the past two years, the Event Horizon Telescope (EHT) collaboration has begun sub-mm observations of a selection of LLAGNs. A handful of the highest priority LLAGN targets are identified as part of the Event Horizon and Environs (ETHER) sample (Ramakrishnan et al. 2021; Ramakrishnan et al. 2023). These select targets have SMBH masses and spins measurable by EHT, and they represent the “next generation” of most likely candidates to display event horizons resolvable by a future expanded EHT array (Johnson et al. 2023; Zhang et al. 2024a). To inform EHT studies and to further explore the accretion and feedback mechanisms of LLAGNs, we conducted an extensive X-ray monitoring campaign of two high priority EHT+multi-wavelength targets: NGC 4594 and IC 1459. Key properties of these sources are reported in Table 1 and summarized below.

NGC 4594 (referred to as Sombrero for the remainder of this work) is a nearby ( $z \sim 0.003$ ) nearly edge-on ( $< 84^\circ$ ) spiral galaxy with a central low-ionization nuclear emission-line region (LINER). It has a two-sided jet/counterjet structure extending from a radio core (Gallimore et al. 2006; Hada et al. 2013; Mezcua & Prieto 2014; Kharb et al. 2016; Yang et al. 2024) that is inclined at  $\sim 66^\circ$  (Yan et al. 2024). Its 230 GHz flux provided in the *ALMA* Source Catalog<sup>1</sup> is 198 mJy (0.198 Jy). The central SMBH has a measured mass in the range of  $6.6 \times 10^8 M_\odot$  (Jardel et al. 2011; Gültekin et al. 2019) –  $1.0 \times 10^9 M_\odot$  (Kormendy 1988; Kormendy et al. 1996). Its event horizon has a predicted angular size of  $\theta_{ring} \sim 7 - 10 \mu\text{as}$  depending on which mass estimate is used; this is large enough to be potentially resolved by EHT in the future. The broadband SED shows evidence for a mid-IR “bump” attributed to thermal emission from a cold and/or truncated accretion disk (Fernández-Ontiveros et al. 2023). Recent measurements of broad mid-IR emission line widths with *JWST* indicate some form of outflow is present, but it is unclear whether this comes from a RIAF-induced wind or jets (there may also be a nuclear dust contribution; see Goold et al. 2024 for further detail). The nucleus appears as a moderately bright X-ray source with some extended emission attributed to hot gas and/or stellar binaries (Li et al. 2010, 2011). Power law fits to *Chandra* (e.g., Pellegrini et al. 2003; González-Martín et al. 2009; Li et al. 2011), *XMM-Newton* (Pellegrini et al. 2003), *BeppoSAX* (Pellegrini et al. 2002), and *ASCA* (Nichol-

<sup>1</sup> <https://almascience.nrao.edu/sc/>

son et al. 1998) spectra from the nucleus generally follow a slope  $\Gamma \sim 2$  (Li et al. 2011).

IC 1459 is a well-studied elliptical galaxy with symmetric jets (Tingay & Edwards 2015) located at  $z \sim 0.006$ . It has a counter-rotating stellar core (Franx & Illingworth 1988), which may suggest it underwent a merger sometime in its past. The central SMBH has a measured mass in the range of  $2.5 - 2.6 \times 10^8 M_\odot$  (Cappellari et al. 2002; Schulze & Gebhardt 2011; Saglia et al. 2016; Gültekin et al. 2019). Its event horizon has a predicted angular size of  $\theta_{ring} \sim 8.9 - 9.0 \mu\text{as}$  depending on which mass estimate is used. Its nucleus contains a strong (1 Jy) compact radio source with a diameter less than  $0.03''$  (Slee et al. 1994) and a hard AGN-like X-ray component (*ASCA*; Matsumoto et al. 1997). The 230 GHz flux is 217 mJy (0.217 Jy; Ruffa et al. 2019) at arcsec scale resolution. The intrinsic nuclear X-ray source has a power law form with fitted slope  $\Gamma \sim 1.9$  combined with a thermal hot gas component with  $kT \sim 0.6$  keV (Fabbiano et al. 2003; Ivey et al. 2024).

The remainder of this manuscript is organized as follows. The X-ray data and analysis strategy to produce spectra and light curves are presented in Section 2. Spectral fitting and light curve variability findings, as well as comparisons to existing literature, are reported in Section 3. In Section 4, we interpret the spectral and variability properties in the context of LLAGN accretion and feedback mechanisms. A final summary and conclusions are presented in Section 5.

## 2. DATA REDUCTION & ANALYSIS

In 2022, we monitored three LLAGN targets of interest to EHT using the *Neutron star Interior Composition ExploreR* (*NICER*, Program Number 5676; Gendreau et al. 2012) telescope at 0.2 – 12 keV energies<sup>2</sup>. This work will focus on the emission characteristics of the two fainter targets – Sombrero and IC 1459 – with the third target (NGC 3998) presented in a future study (Ramakrishnan et al., in prep.). Sombrero was observed from March - August 2022 and IC 1459 was observed from May - October 2022. All sources were observed for 3 ksec every  $\sim 3$  days for each LLAGN during their respective observing windows. A handful of observations for each source had too little exposure and/or too much background noise to be scientifically useful, and are excluded from further analysis. This leaves 49 and 41 usable *NICER* observations for Sombrero and IC 1459, respectively.

<sup>2</sup> *NICER* spectra in the 12 – 15 keV band is almost exclusively used for background modeling.

During the *NICER* X-ray monitoring, we also obtained a snapshot observation of each target with the *Nuclear Spectroscopic Telescope Array* (*NuSTAR*, Program Number 00008229; Harrison et al. 2013) and the *Neil Gehrels Swift Observatory* (*Swift*; Gehrels et al. 2004). The *Swift* observations were performed with all three instruments onboard: the X-ray Telescope (XRT; Burrows et al. 2005), the Ultraviolet/Optical Telescope UVOT; (Roming et al. 2005, 170–600 nm), and the Burst Alert Telescope (BAT; Barthelmy et al. 2005, 15 – 150 keV). In this work, we focus only on the XRT data. A short EHT+*ALMA* observation of Sombrero was also taken during the *NICER* monitoring, and will be the subject of a future study.

All extracted spectra are modeled in the X-ray spectral fitting package *XSPEC* (Arnaud 1996)<sup>3</sup>. Given the faintness of our sources ( $\sim 0.1$  counts/sec in the *NICER* band), we opt to use Cash statistics (Cash 1979) when fitting rather than the classic  $\chi^2$ . Due to low count rates and increased residuals beyond a certain energy threshold, source fluxes are only extracted from fits in the range of: 0.3 – 8 keV for *NICER*, 3 – 20 keV for *NuSTAR*, and 0.3 – 5 keV for *Swift*<sup>4</sup>.

### 2.1. *NICER*

The *NICER* observations are processed using *HEASoft* v6.32.1<sup>5</sup>, starting with the *NICERL2*<sup>6</sup> task. Due to low signal ( $\lesssim 1$  cts  $\text{s}^{-1}$ ), high overshoots ( $> 30$ ), and signatures of background flaring activity present in a significant fraction of the observations, the overshoots (‘overonly’ range) are restricted to  $< 1.5$  for Sombrero and  $< 1.0$  for IC 1459. The undershoots (‘underonly’ range) are kept at the default level  $< 500$ . Overshoots track the non-X-ray high-energy particle backgrounds (e.g., cosmic rays), while undershoots track detector resets due to excess charge from, e.g., optical photons and thermal excitations (LaMarr et al. 2016).

#### 2.1.1. Spectra

Spectra are extracted using the *NICERL3-spec* task, configured with the optimal binning scheme introduced in Kaastra & Bleeker (2016) and a minimum of 10 counts per bin. The background spectra are generated using the *SCORPEON* tool<sup>7</sup> with the ‘script’ setting, which enables adjustable background components that can be

<sup>3</sup> <https://heasarc.gsfc.nasa.gov/xanadu/xspec/>

<sup>4</sup> IC 1459 was too faint to constrain the spectrum beyond the *NICER* band.

<sup>5</sup> <https://heasarc.gsfc.nasa.gov/docs/software/heasoft/>

<sup>6</sup> [https://heasarc.gsfc.nasa.gov/docs/nicer/nicer\\_analysis.html](https://heasarc.gsfc.nasa.gov/docs/nicer/nicer_analysis.html)

<sup>7</sup> [https://heasarc.gsfc.nasa.gov/docs/nicer/analysis\\_threads/scorpeon-overview/](https://heasarc.gsfc.nasa.gov/docs/nicer/analysis_threads/scorpeon-overview/)

Source	Distance (Mpc)	Galactic $N_H$ $10^{20}$ atoms/cm $^2$	$\log M_{\text{BH}}$ ( $M_\odot$ )	Ring Size ( $\mu\text{as}$ )	mm Flux Density (Jy)	Average X-ray flux (erg/cm $^2$ /s)	Inferred $f_{\text{Edd}}$ ( $10^{-5}$ )
M87*	16.8	2.54	9.8	42	1.2	7.3E-12	0.83
<b>Sombrero</b>	9.87	3.67	8.82	7.0	0.2	1.3E-12	1.8
<b>IC 1459</b>	28.92	1.15	9.4	8.9	0.2	1.0E-12	2.4
SgrA*	0.008	110.10	6.6	51.8	2.4	1.8E-13	0.056

**Table 1.** Selection of EHT high priority LLAGN targets shown in bold, sorted in descending order of average 0.3 – 20 keV (*NICER*+*NuSTAR*) X-ray brightness. M87\* and SgrA\* – the two LLAGNs with event horizons already imaged by EHT – are included for comparison purposes, with source properties taken from [Event Horizon Telescope Collaboration et al. \(2019\)](#); [GRAVITY Collaboration et al. \(2019\)](#); [The Event Horizon Telescope Collaboration \(2022\)](#) and references therein. Average X-ray fluxes are taken from the *NASA/IPAC Extragalactic Database*.  $N_H$  values are taken from the *Chandra Galactic Neutral Hydrogen Density Calculator*, which queries the Colden database compiled from [Dickey & Lockman \(1990\)](#). Black hole masses for Sombrero and IC1459 are from [Jardel et al. \(2011\)](#) and [Cappellari et al. \(2002\)](#) and distances are from [Kormendy & Ho \(2013\)](#). Inferred  $f_{\text{Edd}}$  are from [Zhang et al. \(2024b\)](#), see their Section 4.1 for more detail on their calculations.

jointly modeled with the source. The 0.3 – 15 keV energy range is used to facilitate fitting both the background and source models.

The spectra are fit using XSPEC version 12.13.1, with solar abundances from [Wilms et al. \(2000\)](#). The photoelectric absorption cross-sections were taken from [Verner et al. \(1996\)](#). We fix the target galaxies’ redshifts to values taken from the *NASA/IPAC Extragalactic Database (NASA/IPAC Extragalactic Database (NED) 2019)*<sup>8</sup>, and the Galactic absorption  $N_H$  to the values reported in the *Chandra Galactic Neutral Hydrogen Density Calculator (Dickey & Lockman 1990)*<sup>9</sup>. We extract the 2 – 10 keV absorbed fluxes for the combined model components using the XSPEC `cflux` convolution model. Due to increased residuals beyond  $\sim 8$  keV, individual model components’ absorbed fluxes are only extracted in the 0.3 – 8 keV range.

Previous efforts to fit the soft (here defined as 0.3 – 8 keV) X-ray spectra of these sources found that both power law and thermal emission components were needed to describe the spectral shape (e.g., [Fabbiano et al. 2003](#); [Pellegrini et al. 2003](#); [González-Martín et al. 2009](#); [Li et al. 2011](#)). The power law emission may be attributed to inverse Compton scattering of optical/UV disk photons passing through a coronal region<sup>10</sup>. The thermal emission may be attributed to another warm corona of diffuse gas (though, see, e.g., [Kubota & Done 2018](#); [Zoghbi & Miller 2023](#), and references therein for alternative explanations). This thermal component pro-

duces a bump that dominates the emission at  $\lesssim 2$  keV. While more complex thermal (or disk reflection) models could be invoked, we opted for a simple `mekal` component in XSPEC in order to be consistent with several existing studies of these sources. The full model is:

$$\text{tbabs} \times (\text{ztbabs} \times \text{powerlaw} + \text{mekal}) . \quad (1)$$

A representative joint source-background fit is shown in the left panel of Figure 1. The `tbabs` component accounts for absorption from the interstellar medium within our galaxy and should affect all host galaxy emission components. The `ztbabs` component represents the intrinsic local absorption of the nuclear emission by the host galaxy. Both the redshift and the galactic hydrogen column density are fixed to published values for each source (see Table 1). The intrinsic host galaxy absorption is frequently only constrained with an upper limit in our fits – in these situations, we freeze it to the median value from the other observations (reported in Table 2). We find that  $N_H$  is always  $\lesssim 0.1 \times 10^{22}$  atoms/cm $^2$  for Sombrero, and  $\lesssim 2.0 \times 10^{22}$  atoms/cm $^2$  for IC 1459 in our spectral fits.

SCORPEON includes customizable models for both the X-ray and non-X-ray backgrounds. For the majority of our joint source-background fits, we keep all the default SCORPEON parameter settings. In cases where the reduced fit statistic was  $\gtrsim 1.3$  or  $\lesssim 0.9$  and/or the source fit parameters deviate significantly from the general trends, we refit while enabling variations in the constant non-X-ray background (‘CON’), the cosmic ray background (‘COR’), and the lower energy solar wind charge exchange O K and O VII lines.

We estimate the uncertainties on all free parameters and allow refits if new minima are found. If a refit is required, we re-calculate all the uncertainties following the refit. The `steppar` tool is used when non-monotonicity was detected. If any of the SCORPEON terms have uncon-

<sup>8</sup> The NASA/IPAC Extragalactic Database (NED) (<https://ned.ipac.caltech.edu/>) is funded by the National Aeronautics and Space Administration and operated by the California Institute of Technology.

<sup>9</sup> <https://cxc.harvard.edu/toolkit/colden.jsp>

<sup>10</sup> In this context, we interpret corona to mean an X-ray emitting source near the central SMBH, presumed to be made up of a plasma of hot electrons (e.g., [Haardt & Maraschi 1991](#)).

strained uncertainties in the fits, we freeze them back to their defaults and refit.

### 2.1.2. Intra-Day Light Curves

Because `HEASoft` v6.32.1 does not allow `SCORPEON` to be used for background estimation when generating intra-day light curves, we also use the updated v6.33.1 provided on the *SciServer* platform<sup>11</sup> solely to create light curves with the `NICERL3-1c` task including the `SCORPEON` background. We first rerun the `NICERL3-spec` task to generate the appropriate Ancillary Response Files (ARFs) and Response Matrix Files (RMFs) used by `NICERL3-1c` with `SCORPEON`. Light curves are extracted in the 0.3 – 8 keV range with 35 second bins. There is no evidence for significant variability of the source in the intra-day observations, with most fluctuations attributable to variations in the background and accounted for by `SCORPEON`.

### 2.2. *Swift*

*Swift* (0.2–10 keV, 18'' resolution,  $\sim 24'$  field of view) observed both targets quasi-simultaneously with *NuSTAR* during the *NICER* monitoring campaign. A single  $\sim 1$  ks XRT observation was performed in photon counting mode for each target. Spectra were generated using the *Swift*-XRT data product generator tool provided by the UK Swift Science Data Centre (for details, see [Evans et al. 2009](#)), with the iterative centroid option enabled. We applied `ftgrouppha` in the 0.2 – 10 keV range using the same optimal binning scheme used on the *NICER* data, with the exception that we imposed a condition on the required counts per bin to 5 instead of 10.

### 2.3. *NuSTAR*

A single 20 ks *NuSTAR* (3 – 79 keV, 18'' resolution,  $\sim 10'$  field of view) observation was obtained during the *NICER* monitoring campaign for each target. Level 2 and 3 data products were extracted using `nupipeline` and `nuproducts`, respectively, for Focal Plane Modules A and B (FPMA and FPMB). A 50'' region was used to select the source, and a nearby 110'' region was used to select the background. We applied `ftgrouppha` in the 3 – 79 keV range with the same optimal binning scheme used for the *NICER* data (see Section 2.1.1).

### 2.4. Joint *Swift*-*NuSTAR* Fit

The *Swift* and *NuSTAR* observations occurred on the same day for Sombrero, so we perform a joint fit. The quasi-simultaneous *NICER* observation on that day unfortunately had no Good Time Interval (periods when

observing conditions were good), so it was excluded from the joint fit. The observations for IC1459 have insufficient signal for modeling, so we focus the remainder of this section on Sombrero.

For the joint fit, we changed the Eq. 1 model’s power law component to a broken power law, and incorporated a cross-normalization term for each instrument (including *NuSTAR* FPMA and FPMB). The full model is:

$$\text{const} \times \text{tbabs} \times (\text{ztbabs} \times \text{bknpower} + \text{mekal}) . \quad (2)$$

The joint *Swift*-*NuSTAR* fit is shown in the right panel of Figure 1, and the fit parameters are reported in the second column of Table 2. Using the binning described in the previous sections, we are able to fit the 0.3 – 20 keV range. Due to low counts in the *Swift* spectrum, the thermal gas component is difficult to constrain. We therefore opt to freeze its model parameters to the mean values derived from the *NICER* data (see Table 2); the thermal emission appears roughly constant in time, so variability in the parameters **is not** a major concern.

For the joint fit, using a simple power law in place of the broken power law yielded a marginally satisfactory fit (C-statistic/degrees of freedom  $\sim 76/59$ ). Including the break leads to an improvement in the fit statistic ( $\Delta C \sim 20$ ) with the addition of only two free parameters. We additionally perform an F-test to gain a rough estimate of the significance of the post-break  $\Gamma_2$ , finding a chance probability of  $\lesssim 10^{-4}$ . The pre-break  $\Gamma_1$  also agrees nicely with the ( $\Gamma$ ) found in the *NICER* fits (see Table 2), whereas the simple power law  $\Gamma$  skews high ( $\Gamma = 2.3 \pm 0.1$ ). We therefore proceed with the broken power law component in our joint model; the break is interpreted further in Section 4.2.

## 3. RESULTS

We summarize the results of our spectral fits to all observations in Table 2. Example fits to *NICER*, *NuSTAR*, and *Swift* observations of Sombrero are shown in Figure 1. The fitted power law ( $F_{\text{pl}}$ ) and thermal ( $F_{\text{th}}$ ) fluxes from *NICER* are combined to make  $\sim 5$  month light curves for Sombrero and IC 1459. These light curves are shown in Figure 2 and plotted with comparisons to relevant literature fluxes, along with the corresponding power law  $\Gamma$  and thermal  $kT$  from our fits. In this section, we compare the fitted spectra parameters (Table 2) of our two sources with each other and with existing literature, and analyze their variability.

### 3.1. Spectral Modeling: Sombrero

We compare our findings to several existing X-ray studies employing similar power law and thermal emission models. [Pellegrini et al. \(2003\)](#) analyze *XMM-Newton* (40 ks) and *Chandra* observations (18.7 ks) and

<sup>11</sup> <https://apps.sciserver.org/dashboard/>

	Sombrero		IC 1459
	<i>NICER</i>	<i>Swift+NuSTAR</i>	<i>NICER</i> <sup>†</sup>
$\langle\Gamma_1\rangle$	$1.7 \pm 0.4$	$1.6^{+0.3}_{-0.4}$	$2.1 \pm 0.7$
$E_{\text{break}}$ [keV]	–	$6.2^{+1.0}_{-1.7}$	–
$\Gamma_2$	–	$2.9 \pm 0.4$	–
$\langle kT \rangle$ [keV]	$0.5 \pm 0.1$	$0.5^{\dagger\dagger}$	$0.52 \pm 0.09$
$\langle N_H \rangle$ [ $10^{22}$ atoms $\text{cm}^{-2}$ ]	$0.02^{\dagger\dagger\dagger}$	$0.02^{\dagger\dagger\dagger}$	$0.1^{\dagger\dagger\dagger}$
$\langle F_{\text{pl}} \rangle$ [ $10^{-12}$ erg $\text{cm}^{-2} \text{s}^{-1}$ ]	$2.5 \pm 0.9$	$1.14 \pm 0.05$	$0.9 \pm 0.4$
$\langle F_{\text{th}} \rangle$ [ $10^{-12}$ erg $\text{cm}^{-2} \text{s}^{-1}$ ]	$0.25 \pm 0.06$	$< 0.2^{\dagger\dagger\dagger}$	$0.24 \pm 0.04$
$\sigma_{NEV}^2$	$0.12 \pm 0.05$	–	$-0.02 \pm 0.05$

**Table 2.** Source model parameters from fits to the *NICER* and, in the case of Sombrero, joint *Swift+NuSTAR* data. Reported values for *NICER* are the unweighted averages (denoted by brackets) with  $1\sigma$  standard deviation from all observations for all free parameters, and for *Swift+NuSTAR* it is the fitted value and the 90% confidence region for the single observation. We also report the average power law ( $F_{\text{pl}}$ ) and thermal ( $F_{\text{th}}$ ) soft X-ray fluxes (0.3 – 8 keV) and the Normalized Excess Variance ( $\sigma_{NEV}^2$ ) for the power law emission. The thermal emission does not vary enough to produce a meaningful  $\sigma_{NEV}^2$ .

<sup>†</sup>The corresponding *Swift+NuSTAR* snapshot observations have insufficient signal for modeling.

<sup>††</sup>The *Swift+NuSTAR* fit was insensitive to the thermal component, so we freeze  $kT$  to the median value from the *NICER* observations and only estimate an upper limit on  $F_{\text{th}}$ .

<sup>†††</sup>For both LLAGN targets, the majority of the *NICER* fits are insensitive to the intrinsic  $N_H$ ; in these cases, we freeze  $N_H$  to the median value from all fits, and then refit the observations. For *Swift+NuSTAR* we freeze  $N_H$  to the same value as for *NICER*.

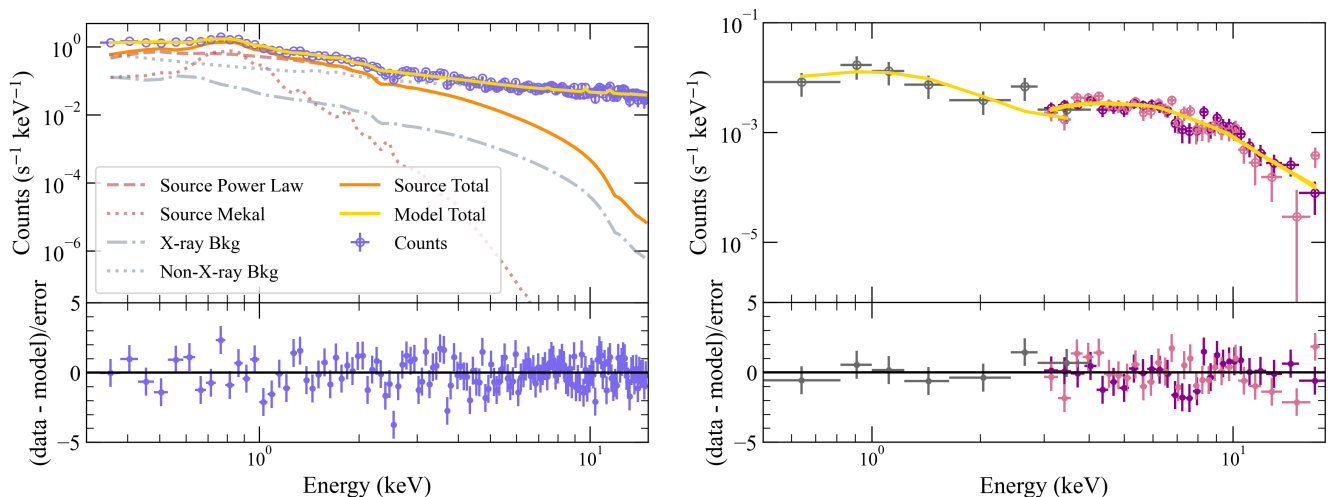


**Figure 1.** *left panel:* Sombrero *NICER* 0.3 – 15 keV spectrum showing counts (blue), source power law component (red dashed line), source mekal component (red dotted line), total source model (Eq. 1; orange line), X-ray background (grey dash-dotted line), non-X-ray background (grey dotted line) and combined source+background models (yellow solid line), generated using SCORPEON and fit in XSPEC. Residuals are shown in the bottom panel. *right panel:* Sombrero joint fit *Swift+NuSTAR* 0.5 – 18 keV background-subtracted source spectrum. *NuSTAR* modules FPMA and FPMB are shown with purple and pink points, respectively, and *Swift* is shown in dark grey. The joint model (Eq. 2; yellow line) and residuals are shown in the bottom panel.

find  $F_{\text{pl}} \sim 2 \pm 0.1 \times 10^{-12}$  erg  $\text{cm}^{-2} \text{s}^{-1}$  (0.5 – 10 keV) and  $\Gamma \approx 1.9$ . González-Martín et al. (2006, 2009) re-analyze the *Chandra* and *XMM-Newton* data. Their best *Chandra* fit is a basic power law with  $F_{\text{pl}}$  comparable to Pellegrini et al. (2003). They report  $\Gamma \approx 1.4$  (González-Martín et al. 2006) and  $\Gamma \approx 1.6$  (González-Martín et al. 2009). For the *XMM-Newton* data they fit a combined power law and thermal model, finding  $\Gamma \approx 2$ . Li et al. (2011) fit all existing *Chandra* observations of Sombrero taken between 1999 and 2008 (includ-

ing those used in Pellegrini et al. 2003 and González-Martín et al. 2006, 2009), finding  $\langle F_{\text{pl}} \rangle \sim 2 \times 10^{-12}$  erg  $\text{cm}^{-2} \text{s}^{-1}$  and  $\Gamma \sim 1.9 \pm 0.1$ . These fluxes are on average comparable to those found in our fits, while  $\Gamma$  is slightly steeper but within one standard deviation of our average. For the thermal component, Pellegrini et al. (2003) find  $F_{\text{th}} \sim 2.6 \pm 0.9 \times 10^{-14}$  erg  $\text{cm}^{-2} \text{s}^{-1}$  (0.5 – 2 keV) and  $kT \sim 0.6$  keV. In the *XMM-Newton* fit by González-Martín et al. (2009), they find comparable fluxes and temperatures. Li et al. (2011) find  $F_{\text{th}}$

is constant at  $\sim 0.2 \times 10^{-12}$  erg cm $^{-2}$  s $^{-1}$  (0.3 – 2 keV) with  $kT \sim 0.58$  keV. Our results agree closely with González-Martín et al. (2006, 2009) and Li et al. (2011), and generally agree with Pellegrini et al. (2003), though their  $F_{\text{th}}$  is slightly lower. Based on the analyses in Li et al. (2010) and Li et al. (2011), the combined flux from non-nuclear discrete X-ray sources should be sub-dominant to  $F_{\text{pl}}$ ;  $F_{\text{th}}$  likely includes a contribution from the discrete sources, but our *NICER* modeling is not sensitive enough to distinguish those components. Additionally, the intrinsic  $N_H$  in all these studies is  $\sim 10^{21}$  atoms/cm $^2$ , which is in agreement with the upper limit of our *NICER* fits, indicating that Sombrero is only moderately absorbed.

In the *Swift*+*NuSTAR* broken power law joint fit of Sombrero, we find a comparable but slightly dimmer  $F_{\text{pl}}$  than the average found with *NICER*. The pre-break  $\Gamma_1$  is essentially the same as the  $\langle \Gamma \rangle$  found with *NICER*, while the post-break  $\Gamma_2$  is steeper. The fit is insensitive to the thermal component, most likely due to low counts (and by extension, wide binning) in the soft X-ray *Swift* observation. We therefore freeze  $kT$  to the median value from the *NICER* observations and only estimate an upper limit on  $F_{\text{th}}$ . Since the thermal component appears roughly constant in the *NICER* observations, freezing it to the median value should not have a significant impact on the fit results. The upper limit from the joint fit falls close to our median  $F_{\text{th}}$  found with *NICER*.

### 3.2. Spectral Modeling: IC 1459

IC1459’s power law emission is roughly half that of Sombrero, but with comparable thermal emission and  $kT$ .  $\langle \Gamma \rangle$  is slightly steeper than what has been found for Sombrero (but with larger uncertainties). The intrinsic  $N_H$  is again  $\sim 10^{21}$  atoms/cm $^2$ , indicating that IC 1459 is also only moderately absorbed.

We compare with a study carried out by Fabbiano et al. (2003): they observe IC 1459 for 60 ks with *Chandra* and find  $F_{\text{pl}} \sim 1.34 \times 10^{-12}$  erg cm $^{-2}$  s $^{-1}$ , while  $F_{\text{th}} \sim 0.03 \times 10^{-12}$  erg cm $^{-2}$  s $^{-1}$ . The power law flux is comparable to ours, while the thermal component is slightly lower. As was the case for Sombrero, Fabbiano et al. (2003) find that the combined flux from non-nuclear discrete X-ray sources should be sub-dominant to  $F_{\text{pl}}$  and  $F_{\text{th}}$ . For the photon index, Fabbiano et al. (2003) find  $\Gamma = 1.88 \pm 0.09$ , while González-Martín et al. (2006, 2009) (refitting the existing *Chandra* data from Fabbiano et al. (2003) and *XMM-Newton* data) find  $\Gamma = 2.17$  (*Chandra*) and  $\Gamma = 1.89$  (*XMM-Newton*). This is also in agreement with our  $\langle \Gamma \rangle$ . Fabbiano et al. (2003) and González-Martín et al. (2006, 2009) both report  $kT \sim 0.6$  keV and  $N_H \sim 10^{21}$  atoms/cm $^2$ , which

agree with our results. Ivey et al. (2024) also re-fit the *XMM-Newton* data; they freeze the power law component to the same parameters as Fabbiano et al. (2003) and instead focus on the thermal component, finding  $kT \sim 0.7$  keV. This is slightly hotter than our inferred temperature, but they also use a different thermal gas model.

### 3.3. Light Curves: Sombrero

Sombrero’s soft X-ray emission seen by *NICER* (left panel of Figure 2) displays a factor of  $\sim 6$  variability in  $F_{\text{pl}}$ , while  $F_{\text{th}}$  (and the corresponding  $kT$ ) stays relatively constant. We detect moments of significant variability beyond what has been reported historically, with a brightening period between MJD 59700 and 59720 being particularly notable (see section 3.6 for further detail). The variability in  $F_{\text{pl}}$  also corresponds to changes in  $\Gamma$ : we find  $\Gamma$  covers a range from  $\sim 0.9 - 2.6$ .

We compare the observed Sombrero *NICER* fluxes in Figure 2 with the historical range of *Chandra* fluxes observed by Li et al. (2011); they find that Sombrero’s nuclear power law emission varies from  $\sim 1.3 - 2.6 \times 10^{-12}$  erg cm $^{-2}$  s $^{-1}$  (a factor of 2)<sup>12</sup>. Historical measurements were taken from a handful of X-ray observations spanning a decade, and so it is not surprising that our dedicated monitoring captures more variation in  $F_{\text{pl}}$  compared to previous works.

### 3.4. Light Curves: IC1459

IC 1459 shows variability in  $F_{\text{pl}}$  to a lesser extent than Sombrero, with a roughly constant  $F_{\text{th}}$  and  $kT$  (right panel of Figure 2).  $F_{\text{pl}}$  varies by a factor of  $\sim 2 - 3$ . The average  $F_{\text{pl}} \approx 10^{-12}$  erg cm $^{-2}$  s $^{-1}$  is consistent with previous *Chandra* observations by Fabbiano et al. (2003). In contrast, Fabbiano et al. (2003) find a significantly lower  $F_{\text{th}}$  (as shown in Figure 2); it is only within the error bars of some of our faintest observations. Fabbiano et al. (2003) do not provide uncertainties on their reported fluxes, but the fact that their fitted  $kT$  is comparable to ours ( $\sim 0.5$  keV) alleviates possible model discrepancy concerns.

### 3.5. Light Curve Variability

We address the light curve variability using the normalized excess variance statistic ( $\sigma_{NEV}^2$ ). It is defined in Nandra et al. (1997) as:

$$\sigma_{NEV}^2 = \frac{1}{N\mu^2} \sum_{i=1}^N [(X_i - \mu)^2 - \sigma_i^2] \quad (3)$$

<sup>12</sup> They simultaneously fit all historical observations with one  $\Gamma$ , so we cannot compare variability in that parameter.

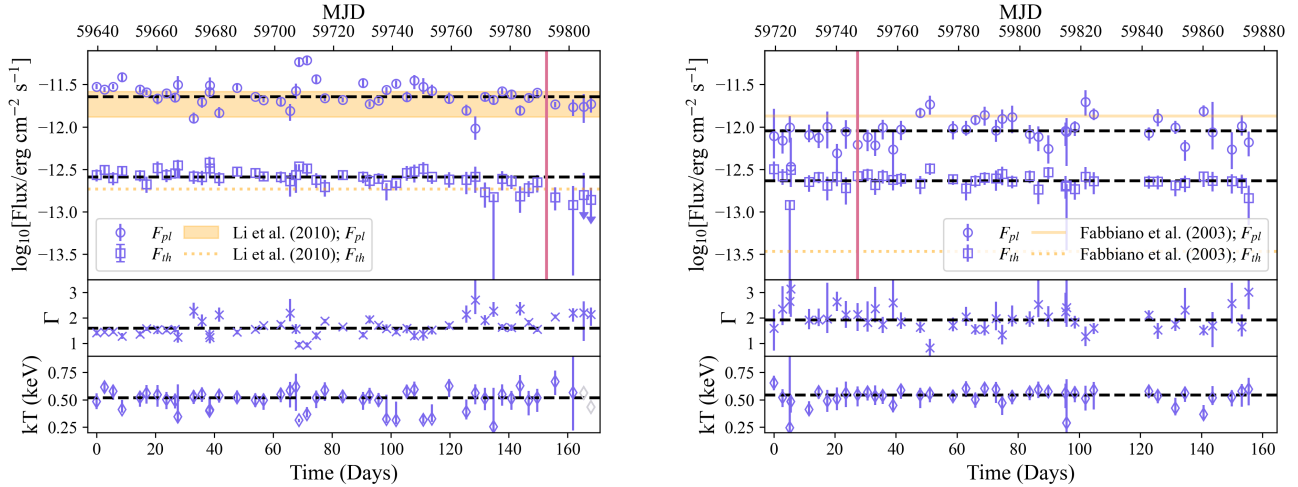


**Figure 2.** Sombrero (left panel) and IC 1459 (right panel) *NICER* 0.3 – 8 keV light curves for  $F_{\text{pl}}$  (blue circles) and  $F_{\text{th}}$  (blue squares) components. These are compared with historical *Chandra* data (orange; power law with solid line, thermal with dashed line) from Li et al. (2011) and Fabbiano et al. (2003) for Sombrero and IC 1459, respectively. The range of Li et al. (2011) *Chandra* Sombrero  $F_{\text{pl}}$  data is denoted as a solid orange region. Corresponding  $\Gamma$  (blue crosses) and  $kT$  (grey diamonds) values are also shown. The last two Sombrero observations have unconstrained  $kT$  (grey diamonds) and the  $F_{\text{th}}$  are therefore marked as upper limits (downward arrows). Median values are shown with black dashed lines. All fitted values are shown with the 90% confidence region. Observation times are reported in Modified Julian Date (top X-axis) and zero-centered days (bottom X-axis). The concurrent *Swift*/*NuSTAR* observation timing is marked with a vertical solid pink line. Both sources show comparable, roughly constant  $F_{\text{th}}$  and  $kT$ , but Sombrero’s  $F_{\text{pl}}$  emission is brighter. Both sources show  $F_{\text{pl}}$  anti-correlated with  $\Gamma$ .

where  $X_i$  is the count rate (or flux) for  $N$  points in the light curve, with errors  $\sigma_i$ , and the unweighted mean count rate (or flux)  $\mu$  (see Nandra et al. 1997 for further discussion of excess variance and estimating its uncertainty). A slightly altered definition is also provided in Vagnetti et al. (2016). We calculate both versions and find them to be equivalent.  $\sigma_{\text{NEV}}^2 = 0.12 \pm 0.05$  for Sombrero and  $-0.02 \pm 0.05$  (consistent with zero variance beyond the flux uncertainties) for IC 1459. In Vagnetti et al. (2016), they estimate  $\sigma_{\text{NEV}}^2$  for a sample of luminous quasars, the dimmest of which is  $L_X \sim 10^{42} \text{ erg s}^{-1}$  (0.5–4.5 keV). For comparison, our LLAGN targets have  $L_X \sim 10^{40} - 10^{41} \text{ erg s}^{-1}$  (0.3–8 keV) using the average soft X-ray fluxes measured from *NICER*<sup>13</sup>. Despite the difference in brightness, Sombrero’s  $\sigma_{\text{NEV}}^2$  is significant and comparable to the values shown in Vagnetti et al. (2016). This also agrees with the findings of Ding et al. (2018): they identify a handful of cosmologically distant ( $z \gtrsim 0.08$ ) LLAGN candidates with  $L_X < 10^{42} \text{ erg s}^{-1}$  (0.5–7 keV) and find  $\sigma_{\text{NEV}}^2 \sim 0.1 - 1$ .

### 3.6. Interplay Between Flux and Spectral Slope

Both Sombrero and IC 1459 show  $\Gamma$  varying inversely with  $F_{\text{pl}}$ . The anti-correlation is highlighted in Figure 3, where we zoom in on the MJD 59700 – 59720 window

and compare the spectra before and during its brightening period. Below  $\sim 2$  keV, the spectral shape stays the same at both times, consistent with  $F_{\text{th}}$  and  $kT$  remaining roughly constant. As  $\Gamma$  increases, however,  $F_{\text{pl}}$  also increases due to enhanced X-ray emission beyond  $\sim 2$  keV. In this energy regime, the emission is dominated by the nuclear power law component rather than the constant thermal component. The same inverse trend appears for the total 2 – 10 keV flux ( $F_{\text{X},2-10\text{keV}}$ ). We quantify the level of anti-correlation by calculating the Spearman’s Rank coefficient  $sp_r$ , provided in Table 3. We find  $sp_r = -0.97$  and  $sp_r = -0.94$  for Sombrero and IC 1459, respectively, with corresponding  $p$  values of  $< 10^{-20}$  for both sources, indicating a very strong  $F_{\text{X},2-10\text{keV}} - \Gamma$  anti-correlation. The anti-correlation, also known as “harder when brighter” behavior, is expected for LLAGNs with certain types of RIAFs, as explained in Younes et al. (2011). We discuss this scenario further in Section 4.1.

## 4. DISCUSSION

### 4.1. Flux-Slope Anti-Correlation

In the LLAGN RIAF scenario, the Eddington ratio  $f_{\text{Edd}} \equiv L_{\text{bol}}/L_{\text{Edd}} \propto L_{\text{X},2-10\text{keV}}/L_{\text{Edd}}$  is inversely proportional to  $\Gamma$  (Gu & Cao 2009). We can convert the *NICER* flux ( $F_{\text{X},2-10\text{keV}}$ ) to a luminosity ( $L_{\text{X},2-10\text{keV}}$ ) and calculate the corresponding  $L_{\text{Edd}}$  using the measured black hole distances and masses provided in Table 1. In Figure 4, we track  $\Gamma$  as a function of

<sup>13</sup> These are fluxes/luminosities absorbed by the host galaxy, but our fitted  $N_H$  are low enough that this should not significantly impact the inferred luminosities.



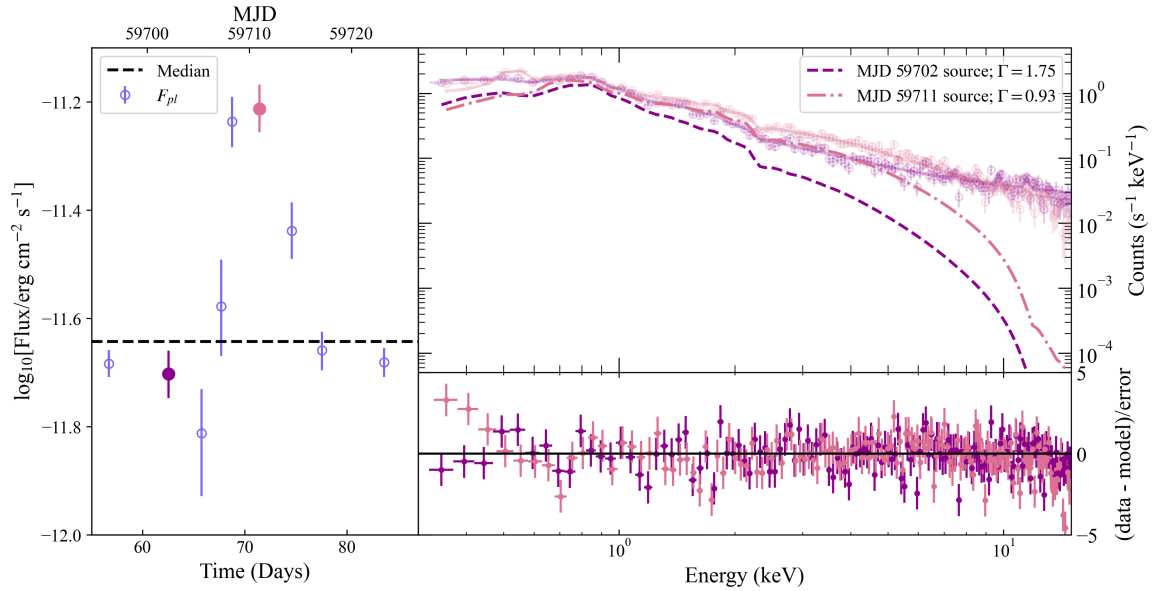


**Figure 3.** Comparison of Sombrero *NICER* spectra before and during a brightening period between MJD 59700 - 59720. *Left panel:* zoomed in light curve tracking  $F_{pl}$  (blue points), with the two highlighted observations shown in purple and pink. The median flux is shown with a dashed black line. *Right panel:* The corresponding spectra for the highlighted observations. Total counts are shown with circles and the fitted source spectra are shown before (purple dashed line) and during the peak brightening (pink dash-dotted line). Residuals are shown at the bottom. As  $F_{pl}$  increases, the spectral shape stays the same below 2 keV, but the  $> 2$  keV slope hardens (i.e.,  $\Gamma$  decreases).

$L_{X,2-10keV}/L_{Edd}$  for Sombrero and IC 1459 as well as several other individual sources and broad surveys from the literature. Given that  $L_{X,2-10keV}$  can be rescaled to  $L_{bol}$  using a roughly constant factor of  $\sim 15 - 20$  for LLAGNs with  $L_{X,2-10keV} \lesssim 10^{42}$  erg s $^{-1}$  (Ho 2008; Younes et al. 2011; Duras et al. 2020), we can treat  $L_{X,2-10keV}/L_{Edd}$  as a proxy for  $f_{Edd}$  without loss of generality. The best fit line to the data tells us about the gradient of the anti-correlation; we use the orthogonal distance regression (ODR) method provided by `scipy` to calculate the best fit taking into account the uncertainties along both axes. Gradient and intercept values and associated uncertainties are provided in Table 3. Both Sombrero and IC 1459 show the expected anti-correlation trend in  $L_{X,2-10keV}/L_{Edd}$ .

This anti-correlation behavior can also be compared with several existing LLAGN studies. We focus our discussion on the very low  $f_{Edd}$  ( $L_{X,2-10keV}/L_{Edd} \lesssim 10^{-5}$ ) regime, since this is where our targets fall and it is the most undersampled  $f_{Edd}$  regime. For examples of “harder when brighter” behavior in higher  $f_{Edd}$  AGNs, see e.g., Emmanoulopoulos et al. (2012); Trakhtenbrot et al. (2017); Diaz et al. (2023); Jana et al. (2023).

First, we consider the Palomar *Swift* observations collected between 2005 and 2014 for the lowest  $f_{Edd}$  sources in Connolly et al. (2016). We select the subset of these AGNs for which Connolly et al. (2016) performed linear

fits: NGC 3031 (M81), NGC 3998, and NGC 3147<sup>14</sup>. These provide the closest comparison with our targets; M81 and NGC 3998 in particular are among the lowest  $f_{Edd}$  and the most well-monitored (in the soft X-ray) LLAGNs to-date. We convert the reported fluxes to  $L_{X,2-10keV}/L_{Edd}$  using distances and masses from Gültekin et al. (2019) and re-fit the *Swift* data using the same fitting routine described above. Our fit results (see Table 3) are comparable to the findings in Connolly et al. (2016). Our sources show similar anti-correlations to NGC 3998, and slightly steeper trends than for M81. Because our sources have even fainter  $L_{X,2-10keV}/L_{Edd}$  than those in Connolly et al. (2016), we can now extend the steep anti-correlation trend seen for individually monitored LLAGNs down to  $\sim 10^{-7-8}$ .

We compare these well-monitored sources with broader LLAGN surveys. Early works by Gu & Cao (2009) and Constantin et al. (2009) find shallow anti-correlation trends from compiled observations of dozens of LINERs and Seyferts assumed to be hosting LLAGNs. Similar behavior is seen in the LLAGN samples from Younes et al. (2011); Hernández-García et al. (2013); Jang et al. (2014); Yang et al. (2015); She et al. (2018). All the individually monitored sources shown in Figure 4

<sup>14</sup> NGC 3147 has only three flux-binned *Swift* data points, making it difficult to confidently fit a linear model. The fit parameters are therefore more uncertain, and the  $spr$  is much lower compared to the other monitored sources (see Table 3).

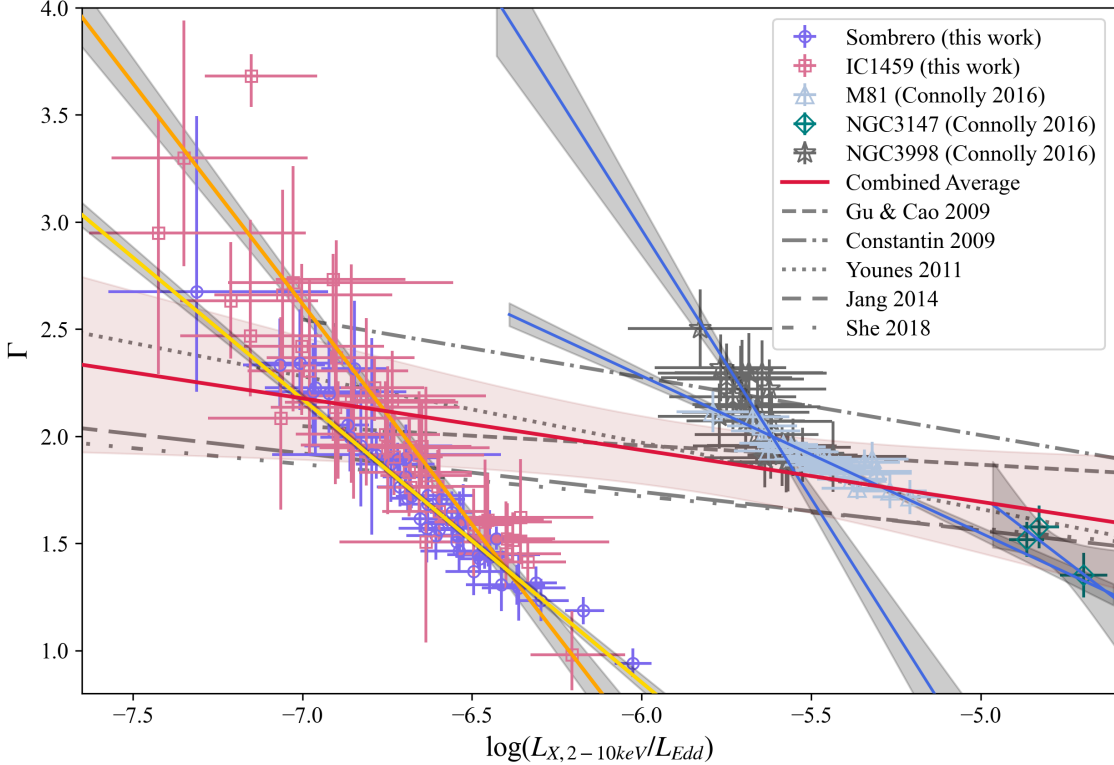


**Figure 4.** Plot of  $\Gamma$  against  $\log(L_{X,2-10keV}/L_{Edd})$  (as a proxy for  $f_{Edd}$ ) for Sombbrero (purple circles), IC 1459 (pink squares), and the lowest  $f_{Edd}$  monitored LLAGNs from Connolly et al. (2016) (M81 with blue triangles, NGC 3998 with grey stars, NGC 3147 with green diamonds). We show our best fit lines and  $1\sigma$  confidence intervals (grey shading) for Sombbrero (yellow solid line), IC 1459 (orange solid line), the other monitored sources (blue solid lines); the best fit parameters are listed in Table 3. We also show the best fits (grey dotted and dashed lines) from several broad LLAGN surveys (Gu & Cao 2009; Constantin et al. 2009; Younes et al. 2011; Jang et al. 2014; She et al. 2018). For comparison with these surveys, we fit a line (red) to the average fluxes of the monitored sources. Sombbrero and IC 1459 are now among the SMBHs with the lowest  $f_{Edd}$  where the  $\Gamma$  anti-correlation is unambiguously detected.

intersect with the best fit lines found by these surveys, though the surveys’ lines have shallower slopes. The shallow slope could be due to the fact that all the survey data comes from snapshot compilations of sources; the best fit survey lines may be more of an “average” fit to a heterogeneous LLAGN sample, with potential systematic scatter in the data caused by observing with different instruments and at different times. This would also explain why the surveys’ observed anti-correlations are often weaker ( $sp_r \lesssim -0.7$ ). A similar situation could explain the minimal slopes found in recent multi-instrument LLAGN sample studies by Jana et al. (2023) and Diaz et al. (2023).

To further investigate this hypothesis, we fit another line to the average fluxes from all the monitored sources. The combined average line (shown in red in Figure 4) matches very closely with all the broad surveys (grey lines). Aggregate samples containing snapshots of many sources therefore seem to wash out the steep anti-correlation trend, which only becomes apparent when monitoring individual LLAGNs. Sombbrero and IC 1459

Object	$\chi^2/\text{DoF}$	Gradient	Intercept	$sp_r$
<b>Sombbrero</b>	0.72	$-1.32 \pm 0.05$	$-7.08 \pm 0.35$	-0.97
<b>IC 1459</b>	1.12	$-2.06 \pm 0.14$	$-11.80 \pm 0.96$	-0.94
M81	0.86	$-0.73 \pm 0.06$	$-2.12 \pm 0.34$	-0.91
NGC3998	0.95	$-2.51 \pm 0.39$	$-12.08 \pm 2.23$	-0.78
NGC3147	0.81	$-1.21 \pm 0.66$	$-4.34 \pm 3.16$	-0.50
Combined Avg.	2.33	$-0.24 \pm 0.19$	$0.49 \pm 1.09$	-0.50

**Table 3.** The reduced  $\chi^2$  and best-fitting parameters (with  $1\sigma$  errors) for linear fits to  $\Gamma$  versus  $\log(L_{X,2-10keV}/L_{Edd})$  for Sombbrero and IC 1459, with M81 *Swift* data from Connolly et al. (2016) included for comparison. The Spearman Rank correlation coefficient ( $sp_r$ ) for each object is also shown.

are now among the lowest  $f_{Edd}$  sources where this anti-correlation is unambiguously detected, and our work verifies the general trends found in other studies of individual sources at higher  $f_{Edd}$  (e.g., Emmanoulopoulos et al. 2012; Connolly et al. 2016; Niu et al. 2023).

The anti-correlation observed for LLAGNs may be due to an increase in the optical depth of the RIAF with in-

creasing mass accretion rate (and by extension, increasing  $L_{X,2-10\text{keV}}$  and  $f_{\text{Edd}}$ ). This leads to an increase in the Compton  $y$ -parameter, which traces how many times photons are being scattered and gaining energy. Increasing this parameter results in a harder X-ray spectrum (smaller  $\Gamma$ ) as photons are bumped up to higher energies (Ho 2009; Gu & Cao 2009; Younes et al. 2011; Niedźwiecki et al. 2015).

Interestingly, theoretical works predict there may be a shift from the X-ray emission being RIAF to jet-dominated below a threshold of  $L_{X,2-10\text{keV}}/L_{\text{Edd}} \sim 10^{-6}$  (Yuan & Cui 2005; Wu et al. 2007; Ho 2008; Yuan et al. 2009; Yang et al. 2015; Connolly et al. 2016; Jana et al. 2023). Yang et al. (2015) in particular claim that the X-rays at  $L_{X,2-10\text{keV}}/L_{\text{Edd}} \lesssim 10^{-6.5}$  come from jet synchrotron emission and the anti-correlation trend should flatten (i.e.,  $\Gamma$  should stay constant) in this lowest  $f_{\text{Edd}}$  regime. We instead find the steep anti-correlation continues below this threshold, extending to at least  $L_{X,2-10\text{keV}}/L_{\text{Edd}} \sim 10^{-7}$ . While we rule out a jet-induced flattening of the anti-correlation trend, it may still be possible for jets to produce the “harder when brighter” behavior if shocks in the jet accelerate electrons and trigger higher energy SSC scatterings (see Connolly et al. 2016; Fernández-Ontiveros et al. 2023 for further discussion). Given that our sources fall very close to the theoretical RIAF/jet-dominated  $f_{\text{Edd}}$  threshold, our *NICER* monitoring data could be used in future detailed broadband SED modeling (see e.g., Hopkins et al. 2009; Bandyopadhyay et al. 2019) to constrain the jet versus RIAF emission contributions.

#### 4.2. Power Law Break

Our best fit power law break occurs at  $\sim 5 - 7$  keV and is flatter pre-break. This type of break has been observed before in AGN, particularly in certain blazars and quasars (e.g., the *NuSTAR*+*Swift* studies in Hayashida et al. 2015; Paliya et al. 2016). These studies both find broken power law fits with flatter pre-break slopes ( $\Gamma_1 \lesssim 1.6$ ,  $\Gamma_2 \gtrsim 1.7$ ) and  $E_{\text{break}} \sim 2 - 10$  keV. They attribute the break to inverse Compton emission via SSC and/or external Compton.

Interestingly, our  $E_{\text{break}}$  is also similar to the results found from fitting *NuSTAR* observations of M87\* during the 2018 EHT campaign (The Event Horizon Telescope-Multi-wavelength science working group et al. 2024). In their case  $E_{\text{break}} \sim 10$  keV, but  $\Gamma_1$  is steeper than  $\Gamma_2$ , whereas we find the reverse. M87\* is a LLAGN like our sources; its properties are summarized in Table 1. In The Event Horizon Telescope-Multi-wavelength science working group et al. (2024), they test multiple broadband SED models for M87\* with and without an X-ray

break. The break appears in their model at the transition region between jet-powered synchrotron and SSC dominating the emission. Sombrero also has jets that dominate the radio/sub-mm emission (see summary in Section 1), but it is unclear how much they contribute to X-ray emission (see Li et al. 2011; Fernández-Ontiveros et al. 2023). Detailed broadband SED modeling for Sombrero using our X-ray data would be useful to constrain the origins of the fitted break, as would deeper observations in the hard X-ray regime.

#### 4.3. Sombrero Variability Timescale

We perform a statistical analysis of Sombrero’s light curve to search for periodicity and the characteristic variability timescale. Due to slight variations in the *NICER* monitoring cadence and removal of poor quality observations, the time between observations ultimately ranges from 0.13 to 6.9 days with an average of 2.9 days. We must therefore employ timing analysis method(s) that can handle data which is unevenly sampled in time. The Lomb-Scargle periodogram is a least-squares method for analyzing unevenly sampled astronomical time series data. It works by iteratively fitting a sinusoidal model to the light curve at a range of frequencies, with a larger power reflecting a better fit at that frequency (VanderPlas 2018). We use the Lomb-Scargle tool provided by `astropy`. but find that the light curve is white noise-dominated and shows no strong evidence for significant periodicity.

The characteristic timescale for aperiodic variability can also be estimated using the correlation function. We use the `pyzdcf` package<sup>15</sup>. It is designed for robust estimation of the cross-correlation – or auto-correlation – function of sparse and unevenly sampled astronomical time-series. We perform an auto-correlation on our Sombrero *NICER* light curve, with the results shown in Figure 5. Inspired by the methods of Hovatta et al. (2007), we identify the peak centered at zero lag. We fit a Gaussian to this peak and estimate its full width half maximum (FWHM): for Sombrero, we find a timescale  $\tau = 6.12$  days. Taking into account the uncertainty on the correlation function amplitudes, which was estimated using 100 Monte-Carlo simulations,  $\tau$  is somewhere between 5 to 7 days. This is close to the predicted Nyquist frequency for our average cadence ( $2 * 2.9$  days  $\sim 5.8$  days), and so any variability timescale below this limit is not well resolved. As seen in Figures 2 and 3, there is a factor of four variability in  $F_{pl}$  on a time scale

<sup>15</sup> `pyzdcf` is a Python module that emulates a widely used Fortran program called ZDCF (Z-transformed discrete Correlation Function, Alexander 1997).

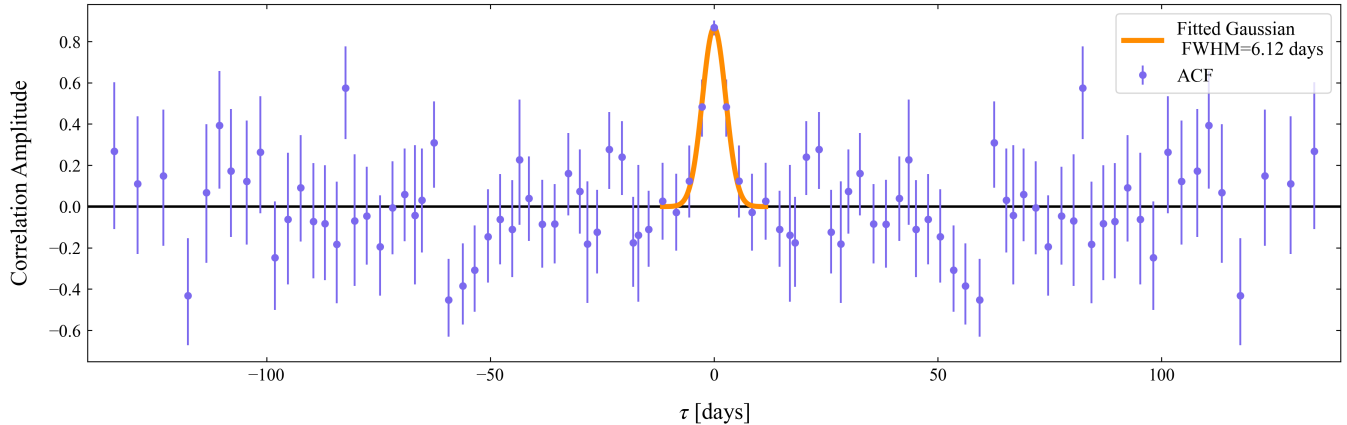


**Figure 5.** Auto-correlation function (ACF) results from the Sombrero *NICER* light curve shown in Figure 2. We consider timescales ranging from 0 - 150 days. The set of non-zero correlation amplitudes (blue points) centered around timescale  $\tau = 0$  are treated as the first peak in the ACF. A Gaussian fit to this peak (orange line) has a full width at half maximum (FWHM)  $\tau = 6.12$  days. This peak width can be interpreted as the shortest variability timescale in the light curve.

faster than 3.5 days. So, significant variability is happening on short timescales  $\lesssim 6$  days, but we can still treat our inferred auto-correlation timescale as an upper limit.

Sombrero’s aperiodic variability timescale is comparable to theoretical predictions for material orbiting at  $< 100r_g$  from the central SMBH. Two of the shortest – and by extension closest to the SMBH – theoretical timescales that we can probe observationally are the light-travel timescale and the free-fall timescale. The light-crossing time is given by

$$\tau_{lc} = \frac{r}{c}. \quad (4)$$

Meanwhile, the radial free-fall timescale for the simplified case of spherical adiabatic Bondi accretion is:

$$\tau_{ff} \approx \left(\frac{r^3}{GM}\right)^{1/2}. \quad (5)$$

For Sombrero’s central SMBH (see Table 1 for source properties) at  $r_{ISCO}$  (innermost stable circular orbit;  $3r_g$  for a non-spinning BH), we find  $\tau_{lc} \sim 0.2$  days and  $\tau_{ff} \sim 0.6$  days. If we equate the 6 day auto-correlation timescale with  $\tau_{lc}$  or  $\tau_{ff}$  and solve for  $r$ , this corresponds to  $r_{lc} \sim 78r_g$  and  $r_{ff} \sim 15r_g$ . We are therefore not able to probe the ISCO with our data, but we do see variability on rapid timescales corresponding to an emission region with  $r < 100r_g$ . In a study by Yan et al. (2024), they report an observed 88 GHz nuclear core size of  $\sim 25 \pm 5 r_g$  – on the same order of magnitude as our inferred  $r_{lc}$  and  $r_{ff}$  – that is consistent with their model predictions from an Advection Dominated Accretion Flow (ADAF). They also fit Sombrero’s broadband SED with a coupled ADAF-jet model and find that the

ADAF dominates at both sub-mm and X-ray frequencies.

## 5. CONCLUSIONS

In this study, we perform X-ray monitoring of two LLAGNs, Sombrero and IC 1459. We use *NICER* to track variations in the soft X-ray emission, and demonstrate *NICER*’s joint source-background modeling capabilities to analyze very faint AGNs in combination with *NuSTAR* and *Swift*. From these observations we find:

1. Both sources are generally described by a combination of power law and thermal components. The average spectral fit parameters agree with literature values for both targets, with Sombrero’s power law emission being slightly brighter than IC 1459’s. Both sources have a thermal component with a temperature of  $\sim 0.5$  keV, with IC 1459 having a slightly softer power law photon index  $\Gamma$  than Sombrero ( $\langle \Gamma \rangle = 2.1$  and 1.7, respectively).
2. For Sombrero, there is tentative evidence for a spectral break in the *NuSTAR* data at  $\sim 6$  keV. This is similar to findings for several other AGNs, where it could correspond to synchrotron/inverse Compton emission in the soft X-ray band.
3. Sombrero shows a factor of  $\sim 6$  flux variability in the power law emission, significantly more than what has been seen historically. The variability shows a characteristic timescale of  $\lesssim 5 - 7$  days. The variability timescale indicates the nuclear X-ray emission likely originates at  $< 100r_g$ .
4. Both Sombrero and IC1459 are “harder when brighter”. They are among the lowest  $f_{Edd}$

sources to exhibit this behavior. This steep anti-correlation trend appears in several other well-monitored LLAGNs. If all of these sources'  $\langle\Gamma\rangle$  and  $\langle L_X/L_{Edd}\rangle$  are fit together, the anti-correlation trend becomes much shallower, as seen in many previous LLAGN surveys.

Coordinated multi-wavelength monitoring of LLAGNs is essential to search for correlated variability and constrain the emission region properties. As we demonstrate in this work, Sombrero is of particular interest due to its significant variability and soft X-ray brightness sufficient for monitoring with *NICER*. IC 1459 also shows interesting  $\Gamma$  anti-correlation behavior, and may be a more suitable target for other X-ray instruments such as *XMM-Newton* and *Chandra*. Future EHT observations of both these LLAGNs provide an urgent motivation for coordinated monitoring, since both submm and X-ray bands are predicted to be either RIAF-dominated or have comparable jet-RIAF contributions (Yan et al. 2024). Meanwhile, upcoming deeper *NuSTAR*+*NICER* observations (PI: N. M. Ford, PID 10244) will help constrain the spectral break(s) while revealing any changes in the hard X-ray emission. Given the level of variability seen in Sombrero with *NICER*, quasi-simultaneous multi-wavelength observations will be essential to inform future time-resolved broadband SED studies aimed at disentangling jet versus RIAF emission contributions. Expanding high-cadence monitoring to a sample of LLAGNs with instruments such as *NICER* will be a crucial next step in characterizing both the variability and the SED shape, and determining how different AGN physical properties (e.g., black hole mass, Eddington ratio, absorption/obscuration) impact the observed emission.

#### ACKNOWLEDGMENTS

NMF is from O'ahu, one of the islands of Hawai'i, an indigenous space where the descendants of the original people are k̄ānaka 'ōiwi / Native Hawaiian. NMF is a visitor in Tiohtiá:ke / Mooniyang, also called Montréal, which lies on the unceded lands of the Kanien'kehá:ka.

We are grateful to the traditional stewards of the lands, waters, and skies that we gather within. As we engage in astronomy on these lands, we respect, listen to, and make space for indigenous voices and ways of knowing the sky and Earth that sustain us all.

This research has made use of the NASA/IPAC Extragalactic Database (NED), which is funded by the National Aeronautics and Space Administration and operated by the California Institute of Technology.

The authors gratefully acknowledge Neil Nagar for his work in defining a sample of high priority EHT targets. We also thank Sera Markoff and Ruby Duncan for their insights into the theoretical modeling of LLAGN broadband SEDs and emission mechanisms. The authors appreciate Craig Markwardt for his development of the SCORPEON background model and for his guidance on applying SCORPEON to our data.

NMF and DH acknowledge funding from the Natural Sciences and Engineering Research Council of Canada (NSERC) Discovery Grant program and the Canada Research Chairs (CRC) program. NMF acknowledges funding from the Fondes de Recherche Nature et Technologies (FRQNT) Doctoral research scholarship. NMF and DH acknowledge support from the Canadian New Frontiers in Research Fund (NFRF) – Explorations program and the Trottier Space Institute at McGill. The authors acknowledge support from the Centre de recherche en astrophysique du Québec, un regroupement stratégique du FRQNT. VR acknowledges the financial support from the visitor and mobility program of the Finnish Centre for Astronomy with ESO (FINCA), funded by the Academy of Finland grant number 306531. DGN acknowledges funding from ANID through Fondecyt Postdoctorado (project code 3220195) and Nucleo Milenio TITANs (project NCN2022002).

*Facilities:* *NICER*, *NuSTAR*, *Swift* (XRT)

*Software:* *astropy* (Astropy Collaboration et al. 2013, 2018, 2022), *scipy* (Virtanen et al. 2020), *HEASoft*, *XSPEC* (Arnaud 1996)

#### APPENDIX

##### A. NICER SPECTRAL FITTING RESULTS



ObsID	$F_{\text{pl}}^\dagger$	$F_{\text{th}}^\dagger$	$F_{X,2-10\text{keV}}$	$\Gamma$	$kT$	$N_H^{\dagger\dagger}$	C-stat	DoF	Reduced
	$\log[\text{Flux}/\text{erg cm}^{-2} \text{ s}^{-1}]$				[keV]	$[10^{22} \text{ atoms cm}^{-2}]$			C-stat
5676010101	-12.11 <sup>+0.27</sup> <sub>-0.32</sub>	-12.50 <sup>+0.14</sup> <sub>-0.09</sub>	-12.14 <sup>+0.38</sup> <sub>-0.35</sub>	1.59 <sup>+0.87</sup> <sub>-0.75</sub>	0.65 <sup>+0.06</sup> <sub>-0.07</sub>	-	128	115	1.12
5676010201	-12.16 <sup>+0.15</sup> <sub>-0.13</sub>	-12.58 <sup>+0.10</sup> <sub>-0.08</sub>	-12.51 <sup>+0.21</sup> <sub>-0.18</sub>	2.35 <sup>+0.63</sup> <sub>-0.89</sub>	0.52 <sup>+0.09</sup> <sub>-0.07</sub>	0.12 <sup>+0.09</sup> <sub>-0.15</sub>	139	121	1.16
5676010301	-12.00 <sup>+0.18</sup> <sub>-0.13</sub>	-12.92 <sup>+1.76</sup> <sub>-0.04</sub>	-12.42 <sup>+0.21</sup> <sub>-0.16</sub>	2.65 <sup>+0.48</sup> <sub>-0.82</sub>	0.24 <sup>+0.11</sup> <sub>-0.87</sub>	0.16 <sup>+0.08</sup> <sub>-0.23</sub>	117	103	1.14
5676010302	-12.47 <sup>+0.24</sup> <sub>-0.34</sub>	-12.50 <sup>+0.16</sup> <sub>-0.06</sub>	-12.66 <sup>+0.16</sup> <sub>-0.15</sub>	3.14 <sup>+1.10</sup> <sub>-2.86</sub>	0.48 <sup>+0.10</sup> <sub>-0.06</sub>	1.04 <sup>+0.57</sup> <sub>-2.01</sub>	135	116	1.17
5676010501	-12.09 <sup>+0.09</sup> <sub>-0.12</sub>	-12.65 <sup>+0.12</sup> <sub>-0.08</sub>	-12.24 <sup>+0.11</sup> <sub>-0.10</sub>	1.91 <sup>+0.36</sup> <sub>-0.44</sub>	0.41 <sup>+0.05</sup> <sub>-0.08</sub>	0.08 <sup>+0.06</sup> <sub>-0.08</sub>	152	126	1.21
5676010601	-12.13 <sup>+0.12</sup> <sub>-0.06</sub>	-12.59 <sup>+0.07</sup> <sub>-0.06</sub>	-12.40 <sup>+0.14</sup> <sub>-0.13</sub>	1.92 <sup>+0.25</sup> <sub>-0.45</sub>	0.57 <sup>+0.07</sup> <sub>-0.04</sub>	0.04 <sup>+0.04</sup> <sub>-0.08</sub>	159	123	1.30
5676010701	-12.00 <sup>+0.26</sup> <sub>-0.18</sub>	-12.69 <sup>+0.17</sup> <sub>-0.11</sub>	-12.32 <sup>+0.28</sup> <sub>-0.25</sub>	1.96 <sup>+0.56</sup> <sub>-1.42</sub>	0.49 <sup>+0.10</sup> <sub>-0.10</sub>	0.10 <sup>+0.09</sup> <sub>-0.38</sub>	119	123	0.97
5676010801	-12.31 <sup>+0.24</sup> <sub>-0.11</sub>	-12.59 <sup>+0.11</sup> <sub>-0.08</sub>	-12.72 <sup>+0.18</sup> <sub>-0.19</sub>	2.63 <sup>+0.37</sup> <sub>-0.39</sub>	0.51 <sup>+0.10</sup> <sub>-0.11</sub>	-	191	137	1.40
5676010901	-12.05 <sup>+0.20</sup> <sub>-0.13</sub>	-12.72 <sup>+0.19</sup> <sub>-0.12</sub>	-12.36 <sup>+0.25</sup> <sub>-0.23</sub>	2.11 <sup>+0.51</sup> <sub>-0.65</sub>	0.56 <sup>+0.13</sup> <sub>-0.11</sub>	0.07 <sup>+0.06</sup> <sub>-0.16</sub>	117	134	0.88
5676011001	-12.21 <sup>+0.29</sup> <sub>-0.22</sub>	-12.58 <sup>+0.12</sup> <sub>-0.09</sub>	-12.41 <sup>+0.24</sup> <sub>-0.26</sub>	2.13 <sup>+0.54</sup> <sub>-0.45</sub>	0.55 <sup>+0.11</sup> <sub>-0.07</sub>	-	143	135	1.06
5676011101	-12.12 <sup>+0.17</sup> <sub>-0.09</sub>	-12.56 <sup>+0.08</sup> <sub>-0.06</sub>	-12.36 <sup>+0.19</sup> <sub>-0.15</sub>	1.83 <sup>+0.37</sup> <sub>-0.82</sub>	0.57 <sup>+0.07</sup> <sub>-0.05</sub>	0.08 <sup>+0.07</sup> <sub>-0.18</sub>	135	125	1.08
5676011201	-12.22 <sup>+0.12</sup> <sub>-0.16</sub>	-12.68 <sup>+0.12</sup> <sub>-0.07</sub>	-12.49 <sup>+0.23</sup> <sub>-0.21</sub>	2.37 <sup>+0.55</sup> <sub>-0.85</sub>	0.53 <sup>+0.08</sup> <sub>-0.10</sub>	0.15 <sup>+0.09</sup> <sub>-0.13</sub>	137	130	1.06
5676011301	-12.01 <sup>+0.14</sup> <sub>-0.09</sub>	-12.58 <sup>+0.09</sup> <sub>-0.07</sub>	-12.26 <sup>+0.17</sup> <sub>-0.12</sub>	1.75 <sup>+0.34</sup> <sub>-0.29</sub>	0.54 <sup>+0.08</sup> <sub>-0.05</sub>	-	180	133	1.36
5676011401	-12.27 <sup>+0.28</sup> <sub>-0.22</sub>	-12.62 <sup>+0.13</sup> <sub>-0.09</sub>	-12.19 <sup>+0.10</sup> <sub>-0.09</sub>	2.60 <sup>+2.13</sup> <sub>-2.73</sub>	0.45 <sup>+0.06</sup> <sub>-0.09</sub>	0.30 <sup>+0.27</sup> <sub>-1.08</sub>	134	114	1.18
5676011501	-12.03 <sup>+0.13</sup> <sub>-0.10</sub>	-12.61 <sup>+0.09</sup> <sub>-0.07</sub>	-12.19 <sup>+0.17</sup> <sub>-0.14</sub>	1.86 <sup>+0.29</sup> <sub>-0.36</sub>	0.59 <sup>+0.08</sup> <sub>-0.05</sub>	0.09 <sup>+0.05</sup> <sub>-0.09</sub>	120	115	1.05
5676011701	-11.83 <sup>+0.05</sup> <sub>-0.06</sub>	-12.67 <sup>+0.12</sup> <sub>-0.09</sub>	-11.97 <sup>+0.18</sup> <sub>-0.15</sub>	1.64 <sup>+0.24</sup> <sub>-0.21</sub>	0.54 <sup>+0.12</sup> <sub>-0.07</sub>	-	127	119	1.07
5676011801	-11.73 <sup>+0.12</sup> <sub>-0.10</sub>	-12.49 <sup>+0.08</sup> <sub>-0.06</sub>	-11.71 <sup>+0.14</sup> <sub>-0.12</sub>	0.83 <sup>+0.33</sup> <sub>-0.35</sub>	0.56 <sup>+0.08</sup> <sub>-0.05</sub>	-	114	118	0.97
5676012001	-12.02 <sup>+0.13</sup> <sub>-0.09</sub>	-12.61 <sup>+0.07</sup> <sub>-0.05</sub>	-12.10 <sup>+0.21</sup> <sub>-0.09</sub>	1.70 <sup>+0.23</sup> <sub>-0.32</sub>	0.53 <sup>+0.05</sup> <sub>-0.06</sub>	0.09 <sup>+0.05</sup> <sub>-0.08</sub>	125	126	0.99
5676012201	-12.03 <sup>+0.07</sup> <sub>-0.10</sub>	-12.73 <sup>+0.14</sup> <sub>-0.10</sub>	-12.15 <sup>+0.11</sup> <sub>-0.10</sub>	2.05 <sup>+0.35</sup> <sub>-0.39</sub>	0.60 <sup>+0.08</sup> <sub>-0.07</sub>	0.12 <sup>+0.07</sup> <sub>-0.07</sub>	142	128	1.11
5676012301	-11.92 <sup>+0.06</sup> <sub>-0.05</sub>	-12.63 <sup>+0.08</sup> <sub>-0.06</sub>	-12.00 <sup>+0.09</sup> <sub>-0.08</sub>	1.56 <sup>+0.22</sup> <sub>-0.19</sub>	0.50 <sup>+0.08</sup> <sub>-0.06</sub>	-	137	120	1.14
5676012401	-11.86 <sup>+0.13</sup> <sub>-0.10</sub>	-12.60 <sup>+0.09</sup> <sub>-0.07</sub>	-11.96 <sup>+0.17</sup> <sub>-0.12</sub>	1.56 <sup>+0.24</sup> <sub>-0.32</sub>	0.60 <sup>+0.08</sup> <sub>-0.05</sub>	0.06 <sup>+0.05</sup> <sub>-0.09</sub>	140	120	1.17
5676012501	-12.04 <sup>+0.13</sup> <sub>-0.13</sub>	-12.61 <sup>+0.14</sup> <sub>-0.09</sub>	-12.16 <sup>+0.17</sup> <sub>-0.15</sub>	1.97 <sup>+0.45</sup> <sub>-0.67</sub>	0.60 <sup>+0.13</sup> <sub>-0.06</sub>	0.18 <sup>+0.11</sup> <sub>-0.16</sub>	130	123	1.06
5676012601	-11.90 <sup>+0.11</sup> <sub>-0.11</sub>	-12.55 <sup>+0.13</sup> <sub>-0.09</sub>	-11.91 <sup>+0.16</sup> <sub>-0.12</sub>	1.34 <sup>+0.38</sup> <sub>-0.39</sub>	0.47 <sup>+0.11</sup> <sub>-0.09</sub>	-	124	117	1.06
5676012701	-11.89 <sup>+0.19</sup> <sub>-0.14</sub>	-12.64 <sup>+0.13</sup> <sub>-0.07</sub>	-12.24 <sup>+0.13</sup> <sub>-0.14</sub>	1.94 <sup>+0.27</sup> <sub>-0.55</sub>	0.53 <sup>+0.07</sup> <sub>-0.06</sub>	0.06 <sup>+0.05</sup> <sub>-0.10</sub>	136	124	1.10
5676012901	-12.09 <sup>+0.11</sup> <sub>-0.11</sub>	-12.58 <sup>+0.08</sup> <sub>-0.06</sub>	-12.29 <sup>+0.10</sup> <sub>-0.11</sub>	1.91 <sup>+0.27</sup> <sub>-0.34</sub>	0.57 <sup>+0.07</sup> <sub>-0.05</sub>	-	163	135	1.21
5676013001	-12.12 <sup>+0.17</sup> <sub>-0.12</sub>	-12.74 <sup>+0.17</sup> <sub>-0.10</sub>	-12.56 <sup>+0.27</sup> <sub>-0.24</sub>	2.53 <sup>+0.50</sup> <sub>-0.96</sub>	0.59 <sup>+0.08</sup> <sub>-0.07</sub>	0.17 <sup>+0.07</sup> <sub>-0.16</sub>	124	136	0.91
5676013101	-12.26 <sup>+0.18</sup> <sub>-0.15</sub>	-12.54 <sup>+0.08</sup> <sub>-0.06</sub>	-12.57 <sup>+0.29</sup> <sub>-0.29</sub>	2.05 <sup>+0.40</sup> <sub>-0.41</sub>	0.58 <sup>+0.06</sup> <sub>-0.05</sub>	-	114	132	0.87
5676013203	-12.05 <sup>+0.18</sup> <sub>-0.10</sub>	-12.70 <sup>+0.15</sup> <sub>-0.12</sub>	-12.41 <sup>+0.27</sup> <sub>-0.18</sub>	2.24 <sup>+0.43</sup> <sub>-0.75</sub>	0.56 <sup>+0.14</sup> <sub>-0.09</sub>	0.12 <sup>+0.07</sup> <sub>-0.14</sub>	129	125	1.04
5676013301	-12.06 <sup>+0.40</sup> <sub>-0.16</sub>	-12.69 <sup>+0.77</sup> <sub>-0.01</sub>	-12.53 <sup>+0.25</sup> <sub>-0.32</sub>	2.40 <sup>+0.76</sup> <sub>-2.45</sub>	0.29 <sup>+0.09</sup> <sub>-0.40</sub>	0.20 <sup>+0.15</sup> <sub>-1.26</sub>	130	107	1.22
5676013401	-12.00 <sup>+0.11</sup> <sub>-0.06</sub>	-12.73 <sup>+0.12</sup> <sub>-0.10</sub>	-12.14 <sup>+0.15</sup> <sub>-0.10</sub>	1.84 <sup>+0.25</sup> <sub>-0.24</sub>	0.56 <sup>+0.08</sup> <sub>-0.06</sub>	-	126	113	1.12
5676013501	-11.71 <sup>+0.16</sup> <sub>-0.14</sub>	-12.58 <sup>+0.15</sup> <sub>-0.11</sub>	-11.86 <sup>+0.18</sup> <sub>-0.16</sub>	1.26 <sup>+0.37</sup> <sub>-0.39</sub>	0.51 <sup>+0.11</sup> <sub>-0.12</sub>	-	152	130	1.17
5676013601	-11.85 <sup>+0.07</sup> <sub>-0.07</sub>	-12.64 <sup>+0.15</sup> <sub>-0.11</sub>	-11.90 <sup>+0.11</sup> <sub>-0.10</sub>	1.59 <sup>+0.23</sup> <sub>-0.21</sub>	0.59 <sup>+0.18</sup> <sub>-0.08</sub>	-	131	112	1.18
5676014201	-12.07 <sup>+0.09</sup> <sub>-0.07</sub>	-12.64 <sup>+0.09</sup> <sub>-0.07</sub>	-12.19 <sup>+0.12</sup> <sub>-0.07</sub>	2.11 <sup>+0.23</sup> <sub>-0.19</sub>	0.58 <sup>+0.06</sup> <sub>-0.05</sub>	-	110	121	0.91
5676014301	-11.90 <sup>+0.10</sup> <sub>-0.11</sub>	-12.64 <sup>+0.09</sup> <sub>-0.07</sub>	-11.84 <sup>+0.08</sup> <sub>-0.07</sub>	1.53 <sup>+0.35</sup> <sub>-0.27</sub>	0.54 <sup>+0.07</sup> <sub>-0.05</sub>	-	135	124	1.09
5676014501	-12.01 <sup>+0.08</sup> <sub>-0.08</sub>	-12.69 <sup>+0.13</sup> <sub>-0.06</sub>	-12.11 <sup>+0.11</sup> <sub>-0.10</sub>	1.74 <sup>+0.26</sup> <sub>-0.25</sub>	0.42 <sup>+0.07</sup> <sub>-0.09</sub>	-	137	131	1.05
5676014601	-12.23 <sup>+0.17</sup> <sub>-0.08</sub>	-12.66 <sup>+0.11</sup> <sub>-0.08</sub>	-12.66 <sup>+0.27</sup> <sub>-0.16</sub>	2.31 <sup>+0.34</sup> <sub>-0.86</sub>	0.56 <sup>+0.08</sup> <sub>-0.06</sub>	0.07 <sup>+0.06</sup> <sub>-0.14</sub>	155	123	1.27
5676014801	-11.82 <sup>+0.07</sup> <sub>-0.07</sub>	-12.58 <sup>+0.12</sup> <sub>-0.06</sub>	-11.89 <sup>+0.08</sup> <sub>-0.07</sub>	1.51 <sup>+0.21</sup> <sub>-0.21</sub>	0.36 <sup>+0.04</sup> <sub>-0.09</sub>	-	128	118	1.09
5676014901	-12.06 <sup>+0.20</sup> <sub>-0.36</sub>	-12.64 <sup>+0.12</sup> <sub>-0.11</sub>	-12.25 <sup>+0.27</sup> <sub>-0.22</sub>	1.69 <sup>+0.85</sup> <sub>-0.54</sub>	0.52 <sup>+0.07</sup> <sub>-0.11</sub>	-	145	131	1.11
5676015101	-12.27 <sup>+0.23</sup> <sub>-0.20</sub>	-12.64 <sup>+0.15</sup> <sub>-0.08</sub>	-12.93 <sup>+0.27</sup> <sub>-0.30</sub>	2.56 <sup>+0.77</sup> <sub>-0.81</sub>	0.52 <sup>+0.08</sup> <sub>-0.06</sub>	0.12 <sup>+0.08</sup> <sub>-0.18</sub>	146	132	1.11
5676015201	-11.99 <sup>+0.11</sup> <sub>-0.13</sub>	-12.66 <sup>+0.13</sup> <sub>-0.10</sub>	-12.00 <sup>+0.14</sup> <sub>-0.12</sub>	1.65 <sup>+0.37</sup> <sub>-0.49</sub>	0.58 <sup>+0.14</sup> <sub>-0.07</sub>	0.08 <sup>+0.07</sup> <sub>-0.12</sub>	126	125	1.01
5676015301	-12.18 <sup>+0.17</sup> <sub>-0.12</sub>	-12.84 <sup>+0.32</sup> <sub>-0.15</sub>	-12.86 <sup>+0.29</sup> <sub>-0.26</sub>	3.01 <sup>+0.67</sup> <sub>-1.07</sub>	0.60 <sup>+0.15</sup> <sub>-0.10</sub>	0.19 <sup>+0.08</sup> <sub>-0.16</sub>	121	132	0.92

**Table 5.** Fitted spectral properties of the *NICER* observations of IC1459.

<sup>†</sup>  $F_{\text{pl}}$  and  $F_{\text{th}}$  are for the 0.3 – 8 keV energy range.

<sup>††</sup> The majority of the fits are insensitive to the intrinsic  $N_H$ ; in these cases, we freeze  $N_H$  to the median value from all fits (see Table 2).

## REFERENCES

- Alexander, T. 1997, in *Astrophysics and Space Science Library*, Vol. 218, *Astronomical Time Series*, ed. D. Maoz, A. Sternberg, & E. M. Leibowitz, 163, doi: [10.1007/978-94-015-8941-3\\_14](https://doi.org/10.1007/978-94-015-8941-3_14)
- Arnaud, K. A. 1996, in *Astronomical Society of the Pacific Conference Series*, Vol. 101, *Astronomical Data Analysis Software and Systems V*, ed. G. H. Jacoby & J. Barnes, 17

- Astropy Collaboration, Robitaille, T. P., Tollerud, E. J., et al. 2013, *A&A*, 558, A33, doi: [10.1051/0004-6361/201322068](https://doi.org/10.1051/0004-6361/201322068)
- Astropy Collaboration, Price-Whelan, A. M., Sipőcz, B. M., et al. 2018, *AJ*, 156, 123, doi: [10.3847/1538-3881/aabc4f](https://doi.org/10.3847/1538-3881/aabc4f)
- Astropy Collaboration, Price-Whelan, A. M., Lim, P. L., et al. 2022, *ApJ*, 935, 167, doi: [10.3847/1538-4357/ac7c74](https://doi.org/10.3847/1538-4357/ac7c74)
- Bandyopadhyay, B., Xie, F.-G., Nagar, N. M., et al. 2019, *MNRAS*, 490, 4606, doi: [10.1093/mnras/stz2874](https://doi.org/10.1093/mnras/stz2874)
- Barthelmy, S. D., Barbier, L. M., Cummings, J. R., et al. 2005, *SSRv*, 120, 143, doi: [10.1007/s11214-005-5096-3](https://doi.org/10.1007/s11214-005-5096-3)
- Best, P. N., & Heckman, T. M. 2012, *MNRAS*, 421, 1569, doi: [10.1111/j.1365-2966.2012.20414.x](https://doi.org/10.1111/j.1365-2966.2012.20414.x)
- Blandford, R. D., & Znajek, R. L. 1977, *MNRAS*, 179, 433, doi: [10.1093/mnras/179.3.433](https://doi.org/10.1093/mnras/179.3.433)
- Burrows, D. N., Hill, J. E., Nousek, J. A., et al. 2005, *SSRv*, 120, 165, doi: [10.1007/s11214-005-5097-2](https://doi.org/10.1007/s11214-005-5097-2)
- Cappellari, M., Verolme, E. K., van der Marel, R. P., et al. 2002, *ApJ*, 578, 787, doi: [10.1086/342653](https://doi.org/10.1086/342653)
- Cash, W. 1979, *ApJ*, 228, 939, doi: [10.1086/156922](https://doi.org/10.1086/156922)
- Chiaberge, M., Gilli, R., Macchetto, F. D., & Sparks, W. B. 2006, *ApJ*, 651, 728, doi: [10.1086/508131](https://doi.org/10.1086/508131)
- Connolly, S. D., McHardy, I. M., Skipper, C. J., & Emmanoulopoulos, D. 2016, *MNRAS*, 459, 3963, doi: [10.1093/mnras/stw878](https://doi.org/10.1093/mnras/stw878)
- Constantin, A., Green, P., Aldcroft, T., et al. 2009, *ApJ*, 705, 1336, doi: [10.1088/0004-637X/705/2/1336](https://doi.org/10.1088/0004-637X/705/2/1336)
- Dermer, C. D., Schlickeiser, R., & Mastichiadis, A. 1992, *A&A*, 256, L27
- Di Matteo, T., Springel, V., & Hernquist, L. 2005, *Nature*, 433, 604, doi: [10.1038/nature03335](https://doi.org/10.1038/nature03335)
- Diaz, Y., Hernández-García, L., Arévalo, P., et al. 2023, *A&A*, 669, A114, doi: [10.1051/0004-6361/202244678](https://doi.org/10.1051/0004-6361/202244678)
- Dickey, J. M., & Lockman, F. J. 1990, *ARA&A*, 28, 215, doi: [10.1146/annurev.aa.28.090190.001243](https://doi.org/10.1146/annurev.aa.28.090190.001243)
- Ding, N., Luo, B., Brandt, W. N., et al. 2018, *The Astrophysical Journal*, 868, 88, doi: [10.3847/1538-4357/aaca60](https://doi.org/10.3847/1538-4357/aaca60)
- Donato, D., Sambruna, R. M., & Gliozzi, M. 2004, *ApJ*, 617, 915, doi: [10.1086/425575](https://doi.org/10.1086/425575)
- Duras, F., Bongiorno, A., Ricci, F., et al. 2020, *A&A*, 636, A73, doi: [10.1051/0004-6361/201936817](https://doi.org/10.1051/0004-6361/201936817)
- Emmanoulopoulos, D., Papadakis, I. E., McHardy, I. M., et al. 2012, *MNRAS*, 424, 1327, doi: [10.1111/j.1365-2966.2012.21316.x](https://doi.org/10.1111/j.1365-2966.2012.21316.x)
- Evans, P. A., Beardmore, A. P., Page, K. L., et al. 2009, *MNRAS*, 397, 1177, doi: [10.1111/j.1365-2966.2009.14913.x](https://doi.org/10.1111/j.1365-2966.2009.14913.x)
- Event Horizon Telescope Collaboration, Akiyama, K., Alberdi, A., et al. 2019, *ApJL*, 875, L1, doi: [10.3847/2041-8213/ab0ec7](https://doi.org/10.3847/2041-8213/ab0ec7)
- Fabbiano, G., Elvis, M., Markoff, S., et al. 2003, *ApJ*, 588, 175, doi: [10.1086/374040](https://doi.org/10.1086/374040)
- Falocco, S., Larsson, J., & Nandi, S. 2020, *A&A*, 638, A67, doi: [10.1051/0004-6361/202037516](https://doi.org/10.1051/0004-6361/202037516)
- Fernández-Ontiveros, J. A., López-López, X., & Prieto, A. 2023, *A&A*, 670, A22, doi: [10.1051/0004-6361/202243547](https://doi.org/10.1051/0004-6361/202243547)
- Franx, M., & Illingworth, G. D. 1988, *ApJL*, 327, L55, doi: [10.1086/185139](https://doi.org/10.1086/185139)
- Gallimore, J. F., Axon, D. J., O’Dea, C. P., Baum, S. A., & Pedlar, A. 2006, *AJ*, 132, 546, doi: [10.1086/504593](https://doi.org/10.1086/504593)
- Gehrels, N., Chincarini, G., Giommi, P., et al. 2004, *ApJ*, 611, 1005, doi: [10.1086/422091](https://doi.org/10.1086/422091)
- Gendreau, K. C., Arzoumanian, Z., & Okajima, T. 2012, in *Society of Photo-Optical Instrumentation Engineers (SPIE) Conference Series*, Vol. 8443, *Space Telescopes and Instrumentation 2012: Ultraviolet to Gamma Ray*, ed. T. Takahashi, S. S. Murray, & J.-W. A. den Herder, 844313, doi: [10.1117/12.926396](https://doi.org/10.1117/12.926396)
- González-Martín, O., Masegosa, J., Márquez, I., Guainazzi, M., & Jiménez-Bailón, E. 2009, *A&A*, 506, 1107, doi: [10.1051/0004-6361/200912288](https://doi.org/10.1051/0004-6361/200912288)
- González-Martín, O., Masegosa, J., Márquez, I., Guerrero, M. A., & Dultzin-Hacyan, D. 2006, *A&A*, 460, 45, doi: [10.1051/0004-6361:20054756](https://doi.org/10.1051/0004-6361:20054756)
- González-Martín, O., Hernández-García, L., Masegosa, J., et al. 2016, *A&A*, 587, A1, doi: [10.1051/0004-6361/201526990](https://doi.org/10.1051/0004-6361/201526990)
- Goold, K., Seth, A., Molina, M., et al. 2024, *ApJ*, 966, 204, doi: [10.3847/1538-4357/ad3065](https://doi.org/10.3847/1538-4357/ad3065)
- GRAVITY Collaboration, Abuter, R., Amorim, A., et al. 2019, *A&A*, 625, L10, doi: [10.1051/0004-6361/201935656](https://doi.org/10.1051/0004-6361/201935656)
- Greene, J. E., & Ho, L. C. 2007, *ApJ*, 667, 131, doi: [10.1086/520497](https://doi.org/10.1086/520497)
- Gu, M., & Cao, X. 2009, *MNRAS*, 399, 349, doi: [10.1111/j.1365-2966.2009.15277.x](https://doi.org/10.1111/j.1365-2966.2009.15277.x)
- Gültekin, K., King, A. L., Cackett, E. M., et al. 2019, *The Astrophysical Journal*, 871, 80, doi: [10.3847/1538-4357/aaf6b9](https://doi.org/10.3847/1538-4357/aaf6b9)
- Haardt, F., & Maraschi, L. 1991, *ApJL*, 380, L51, doi: [10.1086/186171](https://doi.org/10.1086/186171)
- Hada, K., Doi, A., Nagai, H., et al. 2013, *ApJ*, 779, 6, doi: [10.1088/0004-637X/779/1/6](https://doi.org/10.1088/0004-637X/779/1/6)
- Halpern, J. P., & Eracleous, M. 1994, *ApJL*, 433, L17, doi: [10.1086/187537](https://doi.org/10.1086/187537)
- Harrison, F. A., Craig, W. W., Christensen, F. E., et al. 2013, *ApJ*, 770, 103, doi: [10.1088/0004-637X/770/2/103](https://doi.org/10.1088/0004-637X/770/2/103)



- Hayashida, M., Nalewajko, K., Madejski, G. M., et al. 2015, *ApJ*, 807, 79, doi: [10.1088/0004-637X/807/1/79](https://doi.org/10.1088/0004-637X/807/1/79)
- Hernández-García, L., González-Martín, O., Márquez, I., & Masegosa, J. 2013, *A&A*, 556, A47, doi: [10.1051/0004-6361/201321563](https://doi.org/10.1051/0004-6361/201321563)
- Ho, L. C. 2008, *ARA&A*, 46, 475, doi: [10.1146/annurev.astro.45.051806.110546](https://doi.org/10.1146/annurev.astro.45.051806.110546)
- . 2009, *ApJ*, 699, 626, doi: [10.1088/0004-637X/699/1/626](https://doi.org/10.1088/0004-637X/699/1/626)
- Ho, L. C., Feigelson, E. D., Townsley, L. K., et al. 2001, *ApJL*, 549, L51, doi: [10.1086/319138](https://doi.org/10.1086/319138)
- Hopkins, P. F., Hickox, R., Quataert, E., & Hernquist, L. 2009, *MNRAS*, 398, 333, doi: [10.1111/j.1365-2966.2009.15136.x](https://doi.org/10.1111/j.1365-2966.2009.15136.x)
- Hovatta, T., Tornikoski, M., Lainela, M., et al. 2007, *A&A*, 469, 899, doi: [10.1051/0004-6361:20077529](https://doi.org/10.1051/0004-6361:20077529)
- Ivey, L. R., Fabian, A. C., Sanders, J. S., et al. 2024, *MNRAS*, 535, 2697, doi: [10.1093/mnras/stae2516](https://doi.org/10.1093/mnras/stae2516)
- Jana, A., Chatterjee, A., Chang, H.-K., et al. 2023, *MNRAS*, 524, 4670, doi: [10.1093/mnras/stad2140](https://doi.org/10.1093/mnras/stad2140)
- Jang, I., Gliozzi, M., Hughes, C., & Titarchuk, L. 2014, *Monthly Notices of the Royal Astronomical Society*, 443, 72, doi: [10.1093/mnras/stu1024](https://doi.org/10.1093/mnras/stu1024)
- Jardel, J. R., Gebhardt, K., Shen, J., et al. 2011, *ApJ*, 739, 21, doi: [10.1088/0004-637X/739/1/21](https://doi.org/10.1088/0004-637X/739/1/21)
- Johnson, M. D., Akiyama, K., Blackburn, L., et al. 2023, *Galaxies*, 11, 61, doi: [10.3390/galaxies11030061](https://doi.org/10.3390/galaxies11030061)
- Kaasra, J. S., & Bleeker, J. A. M. 2016, *A&A*, 587, A151, doi: [10.1051/0004-6361/201527395](https://doi.org/10.1051/0004-6361/201527395)
- Kawamuro, T., Ueda, Y., Tazaki, F., & Terashima, Y. 2013, *ApJ*, 770, 157, doi: [10.1088/0004-637X/770/2/157](https://doi.org/10.1088/0004-637X/770/2/157)
- Khachikian, E. Y., & Weedman, D. W. 1974, *ApJ*, 192, 581, doi: [10.1086/153093](https://doi.org/10.1086/153093)
- Kharb, P., Srivastava, S., Singh, V., et al. 2016, *MNRAS*, 459, 1310, doi: [10.1093/mnras/stw699](https://doi.org/10.1093/mnras/stw699)
- Kim, D.-W., Anderson, C., Burke, D., et al. 2019, *ApJS*, 241, 36, doi: [10.3847/1538-4365/ab0ca4](https://doi.org/10.3847/1538-4365/ab0ca4)
- Kormendy, J. 1988, *ApJ*, 335, 40, doi: [10.1086/166904](https://doi.org/10.1086/166904)
- Kormendy, J., & Ho, L. C. 2013, *ARA&A*, 51, 511, doi: [10.1146/annurev-astro-082708-101811](https://doi.org/10.1146/annurev-astro-082708-101811)
- Kormendy, J., Bender, R., Ajhar, E. A., et al. 1996, *ApJL*, 473, L91, doi: [10.1086/310399](https://doi.org/10.1086/310399)
- Kubota, A., & Done, C. 2018, *MNRAS*, 480, 1247, doi: [10.1093/mnras/sty1890](https://doi.org/10.1093/mnras/sty1890)
- LaMarr, B., Prigozhin, G., Remillard, R., et al. 2016, in *Space Telescopes and Instrumentation 2016: Ultraviolet to Gamma Ray*, ed. J.-W. A. den Herder, T. Takahashi, & M. Bautz, Vol. 9905, International Society for Optics and Photonics (SPIE), 99054W, doi: [10.1117/12.2232784](https://doi.org/10.1117/12.2232784)
- Li, Z., Spitler, L. R., Jones, C., et al. 2010, *ApJ*, 721, 1368, doi: [10.1088/0004-637X/721/2/1368](https://doi.org/10.1088/0004-637X/721/2/1368)
- Li, Z., Jones, C., Forman, W. R., et al. 2011, *ApJ*, 730, 84, doi: [10.1088/0004-637X/730/2/84](https://doi.org/10.1088/0004-637X/730/2/84)
- Markoff, S., Bower, G. C., & Falcke, H. 2007, *Monthly Notices of the Royal Astronomical Society*, 379, 1519, doi: [10.1111/j.1365-2966.2007.12071.x](https://doi.org/10.1111/j.1365-2966.2007.12071.x)
- Matsumoto, H., Koyama, K., Awaki, H., et al. 1997, *ApJ*, 482, 133, doi: [10.1086/304132](https://doi.org/10.1086/304132)
- Mezcua, M., & Prieto, M. A. 2014, *ApJ*, 787, 62, doi: [10.1088/0004-637X/787/1/62](https://doi.org/10.1088/0004-637X/787/1/62)
- Nagar, N. M., Falcke, H., & Wilson, A. S. 2005, *A&A*, 435, 521, doi: [10.1051/0004-6361:20042277](https://doi.org/10.1051/0004-6361:20042277)
- Nandra, K., George, I. M., Mushotzky, R. F., Turner, T. J., & Yaqoob, T. 1997, *The Astrophysical Journal*, 476, 70, doi: [10.1086/303600](https://doi.org/10.1086/303600)
- Narayan, R. 1996, *ApJ*, 462, 136, doi: [10.1086/177136](https://doi.org/10.1086/177136)
- Narayan, R. 2002, in *Lighthouses of the Universe: The Most Luminous Celestial Objects and Their Use for Cosmology*, ed. M. Gilfanov, R. Sunyaev, & E. Churazov, 405, doi: [10.1007/10856495\\_60](https://doi.org/10.1007/10856495_60)
- NASA/IPAC Extragalactic Database (NED). 2019, *NASA/IPAC Extragalactic Database (NED)*, IPAC, doi: [10.26132/NED1](https://doi.org/10.26132/NED1)
- Nemmen, R. S., Storchi-Bergmann, T., Yuan, F., et al. 2006, *The Astrophysical Journal*, 643, 652, doi: [10.1086/500571](https://doi.org/10.1086/500571)
- Nicholson, K. L., Reichert, G. A., Mason, K. O., et al. 1998, *Monthly Notices of the Royal Astronomical Society*, 300, 893, doi: [10.1111/j.1365-8711.1998.t01-1-01944.x](https://doi.org/10.1111/j.1365-8711.1998.t01-1-01944.x)
- Niedźwiecki, A., Stępnik, A., & Xie, F.-G. 2015, *ApJ*, 799, 217, doi: [10.1088/0004-637X/799/2/217](https://doi.org/10.1088/0004-637X/799/2/217)
- Niu, S., Xie, F.-G., Wang, Q. D., et al. 2023, *MNRAS*, 522, 2644, doi: [10.1093/mnras/stad1080](https://doi.org/10.1093/mnras/stad1080)
- Paliya, V. S., Parker, M. L., Fabian, A. C., & Stalin, C. S. 2016, *ApJ*, 825, 74, doi: [10.3847/0004-637X/825/1/74](https://doi.org/10.3847/0004-637X/825/1/74)
- Pellegrini, S., Baldi, A., Fabbiano, G., & Kim, D.-W. 2003, *The Astrophysical Journal*, 597, 175, doi: [10.1086/378235](https://doi.org/10.1086/378235)
- Pellegrini, S., Fabbiano, G., Fiore, F., Trinchieri, G., & Antonelli, A. 2002, *A&A*, 383, 1, doi: [10.1051/0004-6361:20011482](https://doi.org/10.1051/0004-6361:20011482)
- Prieto, M. A., Fernández-Ontiveros, J. A., Markoff, S., Espada, D., & González-Martín, O. 2016, *Monthly Notices of the Royal Astronomical Society*, 457, 3801, doi: [10.1093/mnras/stw166](https://doi.org/10.1093/mnras/stw166)
- Ptak, A., Terashima, Y., Ho, L. C., & Quataert, E. 2004, *ApJ*, 606, 173, doi: [10.1086/382940](https://doi.org/10.1086/382940)
- Ramakrishnan, V., Chan, C.-K., & Nagar, N. 2021, *Astronomische Nachrichten*, 342, 1180, doi: [10.1002/asna.20210062](https://doi.org/10.1002/asna.20210062)
- Ramakrishnan, V., Nagar, N., Arratia, V., et al. 2023, *Galaxies*, 11, doi: [10.3390/galaxies11010015](https://doi.org/10.3390/galaxies11010015)

- Richards, G. T., Strauss, M. A., Fan, X., et al. 2006, *AJ*, 131, 2766, doi: [10.1086/503559](https://doi.org/10.1086/503559)
- Roming, P. W. A., Kennedy, T. E., Mason, K. O., et al. 2005, *SSRv*, 120, 95, doi: [10.1007/s11214-005-5095-4](https://doi.org/10.1007/s11214-005-5095-4)
- Ruffa, I., Prandoni, I., Laing, R. A., et al. 2019, *Monthly Notices of the Royal Astronomical Society*, 484, 4239, doi: [10.1093/mnras/stz255](https://doi.org/10.1093/mnras/stz255)
- Ruffa, I., Davis, T. A., Elford, J. S., et al. 2024, *MNRAS*, 528, L76, doi: [10.1093/mnras/lsad167](https://doi.org/10.1093/mnras/lsad167)
- Saglia, R. P., Opitsch, M., Erwin, P., et al. 2016, *ApJ*, 818, 47, doi: [10.3847/0004-637X/818/1/47](https://doi.org/10.3847/0004-637X/818/1/47)
- Schawinski, K., Koss, M., Berney, S., & Sartori, L. F. 2015, *MNRAS*, 451, 2517, doi: [10.1093/mnras/stv1136](https://doi.org/10.1093/mnras/stv1136)
- Schmidt, M. 1963, *Nature*, 197, 1040, doi: [10.1038/1971040a0](https://doi.org/10.1038/1971040a0)
- Schulze, A., & Gebhardt, K. 2011, *ApJ*, 729, 21, doi: [10.1088/0004-637X/729/1/21](https://doi.org/10.1088/0004-637X/729/1/21)
- Shakura, N. I., & Sunyaev, R. A. 1973, *A&A*, 24, 337
- She, R., Ho, L. C., Feng, H., & Cui, C. 2018, *The Astrophysical Journal*, 859, 152, doi: [10.3847/1538-4357/aabfe7](https://doi.org/10.3847/1538-4357/aabfe7)
- Sikora, M., Begelman, M. C., & Rees, M. J. 1994, *ApJ*, 421, 153, doi: [10.1086/173633](https://doi.org/10.1086/173633)
- Slee, O. B., Sadler, E. M., Reynolds, J. E., & Ekers, R. D. 1994, *MNRAS*, 269, 928, doi: [10.1093/mnras/269.4.928](https://doi.org/10.1093/mnras/269.4.928)
- The Event Horizon Telescope Collaboration. 2022, *The Astrophysical Journal Letters*, 930, <https://doi.org/10.3847/2041-8213/ac6674>
- The Event Horizon Telescope-Multi-wavelength science working group, The Event Horizon Telescope Collaboration, The Fermi Large Area Telescope Collaboration, et al. 2024, arXiv e-prints, arXiv:2404.17623, doi: [10.48550/arXiv.2404.17623](https://doi.org/10.48550/arXiv.2404.17623)
- Tingay, S. J., & Edwards, P. G. 2015, *Monthly Notices of the Royal Astronomical Society*, 448, 252, doi: [10.1093/mnras/stu2756](https://doi.org/10.1093/mnras/stu2756)
- Trakhtenbrot, B., Ricci, C., Koss, M. J., et al. 2017, *MNRAS*, 470, 800, doi: [10.1093/mnras/stx1117](https://doi.org/10.1093/mnras/stx1117)
- Vagnetti, F., Middei, R., Antonucci, M., Paolillo, M., & Serafinelli, R. 2016, *A&A*, 593, A55, doi: [10.1051/0004-6361/201629057](https://doi.org/10.1051/0004-6361/201629057)
- VanderPlas, J. T. 2018, *The Astrophysical Journal Supplement Series*, 236, 16, doi: [10.3847/1538-4365/aab766](https://doi.org/10.3847/1538-4365/aab766)
- Verner, D. A., Ferland, G. J., Korista, K. T., & Yakovlev, D. G. 1996, *ApJ*, 465, 487, doi: [10.1086/177435](https://doi.org/10.1086/177435)
- Virtanen, P., Gommers, R., Oliphant, T. E., et al. 2020, *Nature Methods*, 17, 261, doi: [10.1038/s41592-019-0686-2](https://doi.org/10.1038/s41592-019-0686-2)
- Willner, S. P., Elvis, M., Fabbiano, G., Lawrence, A., & Ward, M. J. 1985, *ApJ*, 299, 443, doi: [10.1086/163712](https://doi.org/10.1086/163712)
- Wilms, J., Allen, A., & McCray, R. 2000, *ApJ*, 542, 914, doi: [10.1086/317016](https://doi.org/10.1086/317016)
- Wu, Q., Yuan, F., & Cao, X. 2007, *The Astrophysical Journal*, 669, 96, doi: [10.1086/521212](https://doi.org/10.1086/521212)
- Yan, X., Lu, R.-S., Jiang, W., et al. 2024, *ApJ*, 965, 128, doi: [10.3847/1538-4357/ad31a2](https://doi.org/10.3847/1538-4357/ad31a2)
- Yang, Q.-X., Xie, F.-G., Yuan, F., et al. 2015, *MNRAS*, 447, 1692, doi: [10.1093/mnras/stu2571](https://doi.org/10.1093/mnras/stu2571)
- Yang, Y., Li, J.-T., Wiegert, T., et al. 2024, *The Astrophysical Journal*, 966, 213, doi: [10.3847/1538-4357/ad37fd](https://doi.org/10.3847/1538-4357/ad37fd)
- Younes, G., Porquet, D., Sabra, B., & Reeves, J. N. 2011, *A&A*, 530, A149, doi: [10.1051/0004-6361/201116806](https://doi.org/10.1051/0004-6361/201116806)
- Younes, G., Porquet, D., Sabra, B., Reeves, J. N., & Grosso, N. 2012, *A&A*, 539, A104, doi: [10.1051/0004-6361/201118299](https://doi.org/10.1051/0004-6361/201118299)
- Younes, G., Ptak, A., Ho, L. C., et al. 2019, *ApJ*, 870, 73, doi: [10.3847/1538-4357/aaf38b](https://doi.org/10.3847/1538-4357/aaf38b)
- Young, A. J., McHardy, I., Emmanoulopoulos, D., & Connolly, S. 2018, *MNRAS*, 476, 5698, doi: [10.1093/mnras/sty509](https://doi.org/10.1093/mnras/sty509)
- Young, A. J., Nowak, M. A., Markoff, S., Marshall, H. L., & Canizares, C. R. 2007, *ApJ*, 669, 830, doi: [10.1086/521778](https://doi.org/10.1086/521778)
- Yuan, F., & Cui, W. 2005, *ApJ*, 629, 408, doi: [10.1086/431453](https://doi.org/10.1086/431453)
- Yuan, F., Quataert, E., & Narayan, R. 2003, *ApJ*, 598, 301, doi: [10.1086/378716](https://doi.org/10.1086/378716)
- Yuan, F., Yu, Z., & Ho, L. C. 2009, *ApJ*, 703, 1034, doi: [10.1088/0004-637X/703/1/1034](https://doi.org/10.1088/0004-637X/703/1/1034)
- Zhang, X. A., Ricarte, A., Pesce, D. W., et al. 2024a, arXiv e-prints, arXiv:2406.17754, doi: [10.48550/arXiv.2406.17754](https://doi.org/10.48550/arXiv.2406.17754)
- . 2024b, arXiv e-prints, arXiv:2406.17754, doi: [10.48550/arXiv.2406.17754](https://doi.org/10.48550/arXiv.2406.17754)
- Zoghbi, A., & Miller, J. M. 2023, *ApJ*, 957, 69, doi: [10.3847/1538-4357/acfb85](https://doi.org/10.3847/1538-4357/acfb85)